



ELSEVIER

Comput. Methods Appl. Mech. Engrg. 127 (1995) 315–344

**Computer methods
in applied
mechanics and
engineering**

A family of quadrilateral hybrid-Trefftz p -elements for thick plate analysis

J. Jirousek^{a,*}, A. Wróblewski^a, Q.H. Qin^b, X.Q. He^b

^aSwiss Federal Institute of Technology, LSC-DGC, CH-1015 Lausanne, Switzerland

^bHuazhong University of Science and Technology, Wuhan 430074, Hubei, China

Received 16 December 1994

Abstract

This paper presents a family of quadrilateral hybrid-Trefftz (HT) p -elements based on Reissner–Mindlin theory of moderately thick plates. As compared with existing higher-order HT thick plate elements (J. Petrolito), which make use of an incomplete set of polynomial homogeneous solutions for the internal displacement and rotation fields and of an auxiliary conforming frame field involving independently interpolated boundary distributions of displacements and rotations, the new elements differ essentially with respect to the following two points: (1) A T-complete set of homogeneous solutions including polynomial and non-polynomial functions has been derived and used to represent the intraelement displacement and rotations fields. (2) The displacement component of the auxiliary frame field has been linked with the tangential component of the rotation so as to satisfy a particular constraint derived from equilibrium considerations.

The practical efficiency of these modifications has been assessed through a series of numerical examples which have shown that the new p -elements are robust, more accurate in terms of the number of unknowns and of the computational effort, and that they do not lock in the thin limit.

1. Introduction

In the past decade the hybrid-Trefftz (HT) finite element (FE) model, initiated more than fifteen years ago [1, 2], was thoroughly explored and has now become a highly efficient and well-established tool. This model has been successfully applied to various boundary value problems, such as, e.g. plane elasticity [3–5], Kirchhoff plates [6–8], thin shells [9], axisymmetric solid mechanics [10, 11], Poisson's equation [12, 13], etc.

The first application of the HT approach to moderately thick Reissner–Mindlin plates is due to Petrolito [14] who presented a hierarchic family of quadrilateral elements with a number of degrees of freedom (DOF) ranging from 16 to 36. In this standard HT formulation, the displacement and rotation components of the auxiliary frame field $\tilde{\mathbf{u}} = \{\tilde{w}, \tilde{\Theta}_x, \tilde{\Theta}_y\}$, used to enforce conformity on the internal 'Trefftz' field $\mathbf{u} = \{w, \Theta_x, \Theta_y\}$, are independently interpolated along the element boundary in terms of their nodal values.

In a recent paper [15], it has been shown that the performance of the HT thick plate elements can be considerably improved by the application of a linked interpolation whereby the boundary interpolation of the displacement, \tilde{w} , is linked through a suitable constraint with that of the tangential rotation component, $\tilde{\Theta}_t$. This concept, introduced in [16], has recently been applied by several research workers, including the first two authors of the present study, to develop simple and well-performing thick plate

* Corresponding author.

elements [15, 17–22]. In particular, Jirousek et al. [15] has presented a new HT 12 DOF quadrilateral element with quadratic \tilde{w} , linear $\tilde{\Theta}_x$, $\tilde{\Theta}_y$ and an intraelement field \mathbf{u} including 11 polynomial Trefftz functions. As compared with the lowest-order member of the family of standard HT elements of [14]—the DOF element Q21-15S (quadratic \tilde{w} , linear $\tilde{\Theta}_x$, $\tilde{\Theta}_y$, 15 polynomials Trefftz functions)—the linked interpolation used in [15] has not only made it possible to decrease from 16 to 12, the number of DOF and from 15 to 11, the number of Trefftz functions (hence to significantly reduce the cost of computation), but also to increase the solution accuracy if use is made of the same FE mesh.

Practical experience with existing HT elements for thin plates [7, 13], plane elasticity [5] and Poisson's equations [13] has clearly shown that, from the point of view of the cost and the convenience of use, the convergence based on a p -extension is largely preferable to the more conventional h -refinement process [3, 6, 12]. In the HT FE approach the p -extension implies that the representation of the intraelement displacement field is based on a T-complete set of the Trefftz functions [2, 12]. Use of such a set warrants that under very general conditions, the approximation converges towards the exact solution if the number of functions is increased (for a rigorous definition of T-completeness see, e.g. [23]). Unfortunately, the set of polynomial Trefftz functions, as introduced in [14] for thick plate application, is not T-complete and, as a consequence, the convergence of the p -extension process toward the exact solution cannot be warranted. In practice it means that the question of whether the process of increasing the order of approximation of the elements results in improvement or deterioration of the solution is problem dependent. In particular (Section 3), if the tangential component $\tilde{\Theta}_t$ of the rotation at the plate boundary is unconstrained (soft simple support or free edge), then the p -extension may diverge if the internal set of Trefftz functions is not T-complete.

The aim of the present study is threefold:

- to extend the linked interpolation concept, thus far confined to the lowest-order elements, to the higher-order ones;
- to replace the incomplete set of Trefftz functions introduced in [14] by a T-complete set;
- to critically assess the new family of HT thick plate elements based on the aforementioned modifications.

2. Theory

2.1. Basic relations

The family of elements studied in this paper is based on the customary theory of moderately thick plates with transverse shear deformation [24, 25]. A convenient matrix form of the resulting relations of this theory may be obtained through the use (Fig. 1) of the following matrix quantities:

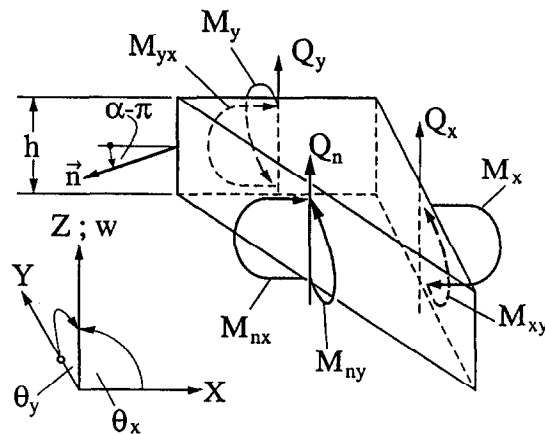


Fig. 1. Displacement, rotations, moments and shear forces involved in generalized vectors \mathbf{u} , $\boldsymbol{\sigma}$ and \mathbf{t} .

$$\mathbf{u} = \{w, \Theta_x, \Theta_y\} \text{ generalized displacement} \tag{1}$$

$$\boldsymbol{\varepsilon} = \{\chi_x, \chi_y, \chi_{xy} \mid \gamma_x, \gamma_y\} = \mathbf{L}\mathbf{u} \text{ generalized strains} \tag{2}$$

$$\boldsymbol{\sigma} = \{M_x, M_y, M_{xy} \mid Q_x, Q_y\} = \mathbf{D}\boldsymbol{\varepsilon} \text{ generalized stresses} \tag{3}$$

$$\mathbf{t} = \{Q_n, -M_{nx}, -M_{ny}\} \text{ generalized boundary tractions} \tag{4}$$

Here

$$\mathbf{L} = \begin{bmatrix} 0 & \partial/\partial x & 0 \\ 0 & 0 & \partial/\partial y \\ 0 & \partial/\partial y & \partial/\partial x \\ \partial/\partial x & -1 & 0 \\ \partial/\partial y & 0 & -1 \end{bmatrix} \text{ strain operator matrix} \tag{2a}$$

$$\mathbf{D} = \begin{bmatrix} \mathbf{D}_M & 0 \\ 0 & \mathbf{D}_S \end{bmatrix} \text{ elasticity matrix} \tag{3a}$$

where

$$\mathbf{D}_M = -\frac{Eh^3}{12(1-\nu^2)} \begin{bmatrix} 1 & \nu & 0 \\ \nu & 1 & 0 \\ 0 & 0 & \frac{1-\nu}{2} \end{bmatrix}, \quad \mathbf{D}_S = Ghk \begin{bmatrix} 1 & 0 \\ 0 & 1 \end{bmatrix}, \tag{3b, c}$$

(E is Young modulus, ν is Poisson's ratio, $G = E/2(1 + \nu)$ is the shear modulus, h is the plate thickness, $k = 5/6$ is the correction factor for non-uniform distribution of shear stress across h) and finally,

$$\mathbf{A} = \left[\begin{array}{ccc|cc} 0 & 0 & 0 & \cos \alpha & \sin \alpha \\ -\cos \alpha & 0 & -\sin \alpha & 0 & 0 \\ 0 & -\sin \alpha & -\cos \alpha & 0 & 0 \end{array} \right] \begin{array}{l} \text{boundary tractions} \\ \text{transformation matrix} \end{array} \tag{4a}$$

The governing differential equations of moderately thick plates are obtained if the differential equilibrium conditions are written in terms of \mathbf{u} as

$$\mathbf{L}^T \boldsymbol{\sigma} = \mathbf{L}^T \mathbf{D} \mathbf{L} \mathbf{u} = -\bar{\mathbf{p}}, \tag{5}$$

where the load vector

$$\bar{\mathbf{p}} = \{\bar{p}, -\bar{m}_x, -\bar{m}_y\} \tag{5a}$$

comprises the distributed vertical load in the z direction and distributed moment loads about the y and x axes (the overhead bar stands for imposed quantities).

2.2. Variational formulation of HT thick plate p -elements

The HT FE model is based on simultaneous use of two independent fields of generalized displacement (Fig. 2)

- a non-conforming ‘Trefftz’ field

$$\mathbf{u} = \hat{\mathbf{u}} + \sum_{i=1}^m N_i c_i = \hat{\mathbf{u}} + \mathbf{N} \mathbf{c} \tag{6}$$

where c_i stands for undetermined coefficients and $\hat{\mathbf{u}}$ and N_i are, respectively, the particular and homogeneous solutions to the governing differential equations (5), namely

$$\mathbf{L}^T \mathbf{D} \mathbf{L} \hat{\mathbf{u}} = -\bar{\mathbf{p}} \quad \text{and} \quad \mathbf{L}^T \mathbf{D} \mathbf{L} N_i = 0 \tag{6a, b}$$

- an exactly and minimally conforming (C^0) auxiliary field

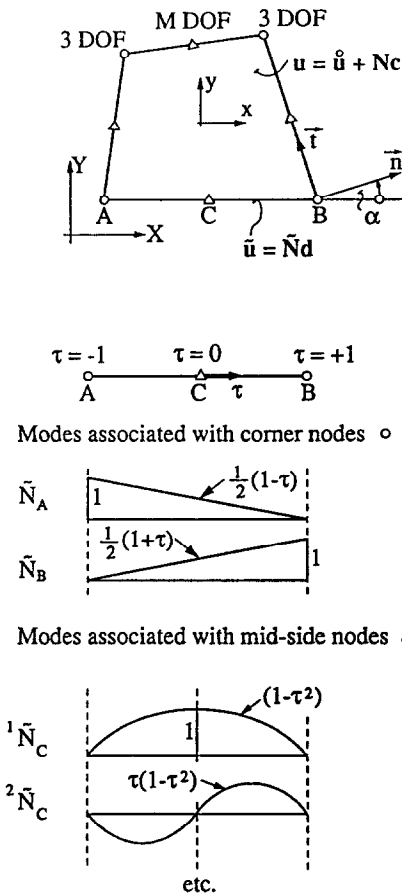


Fig. 2. Typical HT thick plate p -element and its frame functions.

$$\tilde{u} = \tilde{N}d \tag{7}$$

obtained in the customary way in terms of nodal parameters d .

The variational formulation may be based on the following stationary principle [26]

$$H(u, \tilde{u}) = \Pi(\tilde{u}) - \sum_e U^e(\epsilon - \tilde{\epsilon}) = \text{Stationary} \tag{8}$$

where $\Pi(\tilde{u})$ is the total potential energy of the plate expressed in terms of the conforming displacements \tilde{u} , $U^e(\epsilon - \tilde{\epsilon})$ is the strain energy of the difference $\epsilon - \tilde{\epsilon} = L(u - \tilde{u})$ for element e and where the sum \sum_e is taken over all elements of the assembly.

This formulation, which enforces conformity on u and reciprocity on boundary tractions $t = ADLu$ at the interelement boundaries in addition to enforcing the free boundary condition, $t = \bar{t}$ on I_i (for details see [26]), straightforwardly leads to the standard force–displacement relationship

$$r = \hat{r} + kd \tag{9}$$

where r stands for vector of equivalent nodal forces. Here, the load dependent part \hat{r} of r and the symmetric positive definite stiffness matrix k of the element are defined as

$$\hat{r} = g - GH^{-1}h \quad \text{and} \quad k = GH^{-1}G^T \tag{9a, b}$$

where the auxiliary matrices H , h , G and g can be evaluated (see [26]) by performing the following boundary integrals

$$H = \int_{\Gamma^e} T^T N \, d\Gamma = \int_{\Gamma^e} N^T T \, d\Gamma, \quad G = \int_{\Gamma^e} \tilde{N}^T T \, d\Gamma, \tag{10a, b}$$

$$h = \int_{\Gamma^e} T^T \dot{u} \, d\Gamma, \quad g = \int_{\Gamma^e} \tilde{N}^T \dot{t} \, d\Gamma - \int_{\Gamma_f^e} \tilde{N}^T \bar{t} \, d\Gamma. \tag{10c, d}$$

($\Gamma^e = \partial\Omega^e$ —element boundary, Γ_f^e —free part of element boundary). The important consequence of the fact that the integration is confined to the element boundary is that the explicit knowledge of the domain interpolation of the auxiliary conforming field \tilde{u} is not necessary and may be replaced by a suitable boundary interpolation of \tilde{u} (Section 2.4).

Once the element assembly has been solved for nodal parameters, the, until now, undetermined parameters c of the internal field $u = \dot{u} + Nc$ of any element can be evaluated in terms of its nodal parameters d as

$$c = -H^{-1}h + H^{-1}G^T d \tag{11}$$

2.3. Internal field $u = \dot{u} + Nc$

For subsequent considerations, the system of governing equations (5) can conveniently be rewritten as

$$D \left[\frac{\partial^2 \Theta_x}{\partial x^2} + \frac{1}{2}(1-\nu) \frac{\partial^2 \Theta_x}{\partial y^2} + \frac{1}{2}(1+\nu) \frac{\partial^2 \Theta_y}{\partial x \partial y} \right] + C \left(\frac{\partial w}{\partial x} - \Theta_x \right) = 0 \tag{12a}$$

$$D \left[\frac{\partial^2 \Theta_y}{\partial y^2} + \frac{1}{2}(1-\nu) \frac{\partial^2 \Theta_y}{\partial x^2} + \frac{1}{2}(1+\nu) \frac{\partial^2 \Theta_x}{\partial x \partial y} \right] + C \left(\frac{\partial w}{\partial y} - \Theta_y \right) = 0 \tag{12b}$$

$$C \left(\nabla^2 w - \frac{\partial \Theta_x}{\partial x} - \frac{\partial \Theta_y}{\partial y} \right) = -\bar{p} \tag{12c}$$

where

$$D = \frac{Eh^3}{12(1-\nu^2)}, \quad C = \frac{5Eh}{12(1+\nu)} \tag{12d}$$

and where, for the sake of simplicity, vanishing distributed moment loads, $\bar{m}_x = \bar{m}_y = 0$, have been assumed.

The coupling of the governing differential equations (12a–c) makes it difficult to generate a T-complete set of homogeneous solutions for w , Θ_x and Θ_y . To bypass this difficulty, two auxiliary functions, f and g , are introduced such that [27]

$$\Theta_x = \frac{\partial g}{\partial x} + \frac{\partial f}{\partial y} \quad \text{and} \quad \Theta_y = \frac{\partial g}{\partial y} - \frac{\partial f}{\partial x} \tag{13a, b}$$

It should be pointed out that

$$\frac{\partial g_0}{\partial x} + \frac{\partial f_0}{\partial y} = 0 \quad \text{and} \quad \frac{\partial g_0}{\partial y} - \frac{\partial f_0}{\partial x} = 0 \tag{14a, b}$$

are Cauchy–Riemann equations, the solution of which always exists. As a consequence, Θ_x and Θ_y remain unchanged if f and g in (13a, b) are replaced by $f + f_0$ and $g + g_0$. This property will play an important role in the subsequent part of this section.

The solution of Eqs. (14a, b) may be conveniently be expressed in a complex variable form (with $i = \sqrt{-1}$) as

$$f_0 + ig_0 = \Phi(x + iy) \tag{14c}$$

The substitution of (13a, b) into the first two differential equations (12) yields

$$\frac{\partial}{\partial x} [D\nabla^2 g + C(w - g)] + \frac{\partial}{\partial y} \left[\frac{1}{2} D(1 - \nu)\nabla^2 f - Cf \right] = 0 \quad (15a)$$

$$\frac{\partial}{\partial y} [D\nabla^2 g + C(w - g)] - \frac{\partial}{\partial x} \left[\frac{1}{2} D(1 - \nu)\nabla^2 f - Cf \right] = 0 \quad (15b)$$

Now, if the contents of the two brackets are considered as independent generalized variables,

$$A = \left[\frac{1}{2} D(1 - \nu)\nabla^2 f - Cf \right] \quad \text{and} \quad B = [D\nabla^2 g + C(w - g)]$$

we again get a set of Cauchy–Riemann equations

$$\frac{\partial B}{\partial x} + \frac{\partial A}{\partial y} = 0$$

$$\frac{\partial B}{\partial y} - \frac{\partial A}{\partial x} = 0$$

and, in the same manner as in (14c), we can set

$$A + iB = \left[\frac{1}{2} D(1 - \nu)\nabla^2 f - Cf \right] + i[D\nabla^2 g + C(w - g)] = F(x + iy) \quad (15c)$$

This relation is a non-homogeneous equation with independent unknown functions f , g and w . Its solution can be composed of a particular solution and a homogeneous solution. Since $F(x + iy)$ is a harmonic function, it is easy to see that the particular solution can be taken as

$$f + ig = -\frac{1}{C} F(x + iy) \quad \text{and} \quad w = 0 \quad (15d)$$

It is obvious, see (13a, b) and (14a, b), that this solutions leads to $\Theta_x = \Theta_y = w = 0$. Therefore, the particular solution may simply be omitted and we only need to consider the homogeneous part of (15c), namely

$$\frac{1}{2} D(1 - \nu)\nabla^2 f - Cf = 0 \quad \text{and} \quad D\nabla^2 g + C(w - g) = 0.$$

From the second of these equations

$$w = g - \frac{D}{C} \nabla^2 g \quad (16)$$

The substitution of this relation and of the expressions (13a, b) into Eq. (12c) finally leads to

$$D\nabla^4 g + \bar{p} = 0. \quad (17)$$

As a result, we obtain for g and f the following differential equations

$$D\nabla^4 g = -\bar{p} \quad (18)$$

and

$$\nabla^2 f - \lambda^2 f = 0 \quad \text{with} \quad \lambda^2 = (1 - \nu) \frac{10}{h^2} \quad (19)$$

2.3.1. Homogeneous solutions $N_i = \{w_i, \Theta_{xi}, \Theta_{yi}\}$

The relations (18) and (19) are the biharmonic equation and the modified Hemholtz equation, respectively.

A set of homogeneous solutions ($\bar{q} = 0$) of the former is represented by biharmonic polynomials, which may be easily obtained [6] from the following generating sequence

$$\left. \begin{aligned} g_1 &= r^2 & g_2 &= x^2 - y^2 & g_3 &= xy \\ g_{4k} &= r^2 \operatorname{Re} z^k & g_{4k+1} &= r^2 \operatorname{Im} z^k \\ g_{4k+2} &= \operatorname{Re} z^{k+2} & g_{4k+3} &= \operatorname{Im} z^{k+2} \end{aligned} \right\} \quad (k = 1, 2, \dots) \tag{20}$$

where $r^2 = x^2 + y^2$ and where Re and Im denote the real and the imaginary parts of a complex number. A set of homogeneous solutions of the latter may be generated from the following sequence [28]

$$\left. \begin{aligned} f_1 &= I_0(\lambda r) \\ f_{2k} &= I_k(\lambda k) \cos k\varphi, \quad f_{2k+1} = I_k(\lambda k) \sin k\varphi \end{aligned} \right\} \quad (k = 1, 2, \dots)$$

where $\varphi = \arctan(y/x)$ and $I_k(\lambda r)$ is the modified Bessel function of the first kind

$$I_k(\alpha) = \sum_{m=0}^{\infty} \frac{\alpha^{(2m+k)}}{2^{(2m+k)} m! \Gamma(k+m+1)} \quad \text{where } \Gamma(a) = \int_0^{\infty} e^{-s} s^{(a-1)} ds \tag{21a}$$

In agreement with relations (13a, b) and (16), the homogeneous solutions $w_i, \Theta_{xi}, \Theta_{yi}$ are obtained in terms of g 's and f 's as

$$\begin{aligned} w_i &= g - \frac{D}{C} \nabla^2 g \\ \Theta_{xi} &= \frac{\partial g}{\partial x} + \frac{\partial f}{\partial y} \quad \text{and} \quad \Theta_{yi} = \frac{\partial g}{\partial y} - \frac{\partial f}{\partial x} \end{aligned}$$

However, as sets (20) of functions g and (21) of functions f are independent of each other, the submatrices $N_i = \{w_i, \Theta_{xi}, \Theta_{yi}\}$ in (6) will be of either of the two following types

$$N_i = \left\{ \begin{array}{c} g_j - \frac{D}{C} \nabla^2 g_j \\ \frac{\partial g_j}{\partial x} \\ \frac{\partial g_j}{\partial y} \end{array} \right\} \quad \text{or} \quad N_i = \left\{ \begin{array}{c} 0 \\ \frac{\partial f_j}{\partial y} \\ -\frac{\partial f_j}{\partial x} \end{array} \right\} \tag{22a, b}$$

One of the possible methods of relating index i to corresponding j values in (22a, b) is displayed in Table 1. However, many other possibilities exist. It should also be pointed out that successful h -method elements have been obtained [14, 15] with only the polynomial set of homogeneous solutions.

Table 1
Example of a definition of corresponding indexes i and j involved in the generation of homogeneous solutions (22a, b)

i	1	2	3	4	5	6	7	8	9	10	
j in (22a)	1	2	3	4	5	–	6	7	8	9	
j in (22b)	–	–	–	–	–	1	–	–	–	–	

i	11	12	13	14	15	16	17	18	19	20	21	22
j in (22a)	–	–	10	11	12	13	–	–	14	15	16	17
j in (22b)	2	3	–	–	–	–	4	5	–	–	–	–

i	23	24	25	26	27	28	29	30	31	32	33	34	...	etc.
j in (22a)	–	–	18	19	20	21	–	–	22	23	24	25	...	etc.
j in (22b)	6	7	–	–	–	–	8	9	–	–	–	–	...	etc.

2.3.2. Particular solution $\dot{\mathbf{u}} = \{\dot{u}, \dot{\Theta}_x, \dot{\Theta}_y\}$

The effect of various loads can accurately be accounted for by a particular solution of the form

$$\dot{\mathbf{u}} = \begin{Bmatrix} \dot{u} \\ \dot{\Theta}_x \\ \dot{\Theta}_y \end{Bmatrix} = \begin{Bmatrix} \dot{g} - \frac{D}{C} \nabla^2 \dot{g} \\ \frac{\partial \dot{g}}{\partial x} \\ \frac{\partial \dot{g}}{\partial y} \end{Bmatrix} \quad (23)$$

where \dot{g} is a particular solution of Eq. (18). The most useful solutions are

$$\dot{g} = -\bar{p}r^4/64D \quad \text{for a uniform load } \bar{p} = \text{const.} \quad (24a)$$

and

$$\dot{g} = -\bar{P}r_p^2 \ln r_p^2 / 16\pi D \quad \text{for a concentrated load } \bar{P} \quad (24b)$$

where

$$r_p^2 = (x - x_p)^2 + (y - y_p)^2$$

A number of particular solutions for Reissner–Mindlin plates can be found in standard texts, e.g. [29].

2.4. Frame field $\tilde{\mathbf{u}} = \tilde{\mathbf{N}}\mathbf{d}$

Since the evaluation of the element matrices (Section 2.1) only calls for boundary integration, the explicit knowledge of the domain interpolation of the auxiliary conforming field $\tilde{\mathbf{u}}$ is not necessary. As a consequence the boundary distribution of $\tilde{\mathbf{u}}$, referred to as ‘frame function’, is all that is needed.

The elements considered in this paper (Fig. 2) are of the p -type, with 3 standard DOF at corner nodes, e.g.

$$\mathbf{d}_A = \tilde{\mathbf{u}}_A = \{\tilde{w}_A, \tilde{\Theta}_{xA}, \tilde{\Theta}_{yA}\} \quad (25a)$$

$$\mathbf{d}_B = \tilde{\mathbf{u}}_B = \{\tilde{w}_B, \tilde{\Theta}_{xB}, \tilde{\Theta}_{yB}\} \quad (25b)$$

and an optional number, M , of hierarchical DOF associated with mid-side nodes

$$\mathbf{d}_C = \Delta \tilde{\mathbf{u}}_C = \{^1\Delta \tilde{w}_C, ^1\Delta \tilde{\Theta}_{xC}, ^1\Delta \tilde{\Theta}_{yC} | ^2\Delta \tilde{w}_C, ^2\Delta \tilde{\Theta}_{xC}, ^2\Delta \tilde{\Theta}_{yC}, \dots \text{ etc.}\} \quad (25c)$$

Since in the thin limit $\tilde{\Theta}_x = \partial \tilde{w} / \partial x$ and $\tilde{\Theta}_y = \partial \tilde{w} / \partial y$, the order of the polynomial interpolation of \tilde{w} has to be one degree higher than that of $\tilde{\Theta}_x$ and $\tilde{\Theta}_y$ if the resulting element is to be free of shear locking. Hence, if along a particular side $A - C - B$ of the element (Figs. 2 and 3)

$$\tilde{\Theta}_x = \tilde{N}_A \tilde{\Theta}_{xA} + \tilde{N}_B \tilde{\Theta}_{xB} + \sum_{i=1}^{\tilde{p}-1} {}^i \tilde{N}_C {}^i \Delta \tilde{\Theta}_{xC}, \quad (26a)$$

$$\tilde{\Theta}_y = \tilde{N}_A \tilde{\Theta}_{yA} + \tilde{N}_B \tilde{\Theta}_{yB} + \sum_{i=1}^{\tilde{p}-1} {}^i \tilde{N}_C {}^i \Delta \tilde{\Theta}_{yC}, \quad (26b)$$

where \tilde{p} is the polynomial degree of $\tilde{\Theta}_x$ and $\tilde{\Theta}_y$ (the last term in (26a, b) will be missing if $\tilde{p} = 1$), then the proper choice for the displacement interpolation is

$$\tilde{w} = \tilde{N}_A \tilde{w}_A + \tilde{N}_B \tilde{w}_B + \sum_{i=1}^{\tilde{p}} {}^i \tilde{N}_C {}^i \Delta \tilde{w}_C, \quad (26c)$$

The application of these functions for $\tilde{p} = 1$ or $\tilde{p} = 2$ along with 13 or 25 polynomial homogeneous solutions (22a) leads to elements identical to Petrolito’s quadrilaterals Q21-13 and Q32-25 in [14]. One

of the aims of the present paper is to show that the performance of these successful elements can be further improved if \tilde{w} is linked to $\tilde{\Theta}_x$ and $\tilde{\Theta}_y$ in agreement with the following consideration:

Since the stationary principle (8) of Section 2.1 indirectly enforces equilibrium on generalized stresses $\tilde{\sigma}$ corresponding to \tilde{u} , it can be expected that the element performance will be improved if some of the parameters of \tilde{u} are suitably linked so as to satisfy some statistical condition a priori (while preserving the necessary C^0 conformity). This may be accomplished if one observes that at the boundary of a rectangular element the polynomial degree of the shear force \tilde{Q}_t , obtained from moment equilibrium as

$$\tilde{Q}_t = \frac{\partial \tilde{M}_t}{\partial t} + \frac{\partial \tilde{M}_{nt}}{\partial n} \tag{27a}$$

is one degree lower¹ than that derived from the tangential component of the shear deformation, namely

$$\tilde{Q}_t = Gkh \left(\frac{\partial \tilde{w}}{\partial t} - \tilde{\Theta}_t \right) \tag{27b}$$

Thus, the term with the highest polynomial degree, \tilde{p} , in $\partial \tilde{w} / \partial t - \tilde{\Theta}_t$ must be constrained to zero (for more details see e.g. [15]). This leads to the following relations

$$\tilde{p} = 1:$$

$${}^1\Delta \tilde{w}_C = \frac{1}{8} (\tilde{\Theta}_{tB} - \tilde{\Theta}_{tA}) L_{AB} \tag{28a}$$

$$\tilde{p} > 1:$$

$$\tilde{p}\Delta \tilde{w}_C = \frac{1}{2(1+\tilde{p})} \tilde{p}^{-1} \Delta \tilde{\Theta}_{tC} L_{AB} \tag{28b}$$

where L_{AB} is the length of the element side and

$$\tilde{\Theta}_t = -\tilde{\Theta}_x \sin \alpha + \tilde{\Theta}_y \cos \alpha = \frac{1}{L_{AB}} (\tilde{\Theta}_x \Delta x_{BA} + \tilde{\Theta}_y \Delta y_{BA}) \tag{28c}$$

where

$$\Delta x_{BA} = x_B - x_A, \quad \Delta y_{BA} = y_B - y_A \tag{28d}$$

Combining (28a–d) with (26c) finally yields

$$\tilde{p} = 1:$$

$$\tilde{w} = \tilde{N}_A \tilde{w}_A + \tilde{N}_B \tilde{w}_B + \frac{1}{8} {}^1\tilde{N}_C [(\tilde{\Theta}_{xB} - \tilde{\Theta}_{xA}) \Delta x_{BA} + (\tilde{\Theta}_{yB} - \tilde{\Theta}_{yA}) \Delta y_{BA}] \tag{29a}$$

$$\tilde{p} > 1:$$

$$\tilde{w} = \tilde{N}_A \tilde{w}_A + \tilde{N}_B \tilde{w}_B + \sum_{i=1}^{\tilde{p}-1} {}^i\tilde{N}_C {}^i\Delta \tilde{w}_C + \frac{1}{2(1+\tilde{p})} \tilde{p}\tilde{N}_C [\tilde{p}^{-1} \Delta \tilde{\Theta}_{xC} \Delta x_{BA} + \tilde{p}^{-1} \Delta \tilde{\Theta}_{yC} \Delta y_{BA}] \tag{29b}$$

Thus, if (26c) is replaced by (29a) or (29b), the polynomial degree of the \tilde{w} interpolation is maintained ($p_{\tilde{w}} = \tilde{p} + 1$ as compared to $p_{\tilde{\sigma}} = \tilde{p}$) while the number M of hierarchical parameters of each element side is reduced by one and is now equal to

$$M = 3(\tilde{p} - 1) \tag{30}$$

¹ Though the domain interpolation of \tilde{u} , necessary for evaluation of the relation (27a), is not given here explicitly, it is easy to see that for $\tilde{p} = 2$, for example, the rotation will be represented by a full quadratic polynomial plus the terms x^2y and xy^2 and the displacement will be a full cubic polynomial plus the terms x^3y and xy^3 .

It should also be noted that the above interpolation not only preserves the necessary C^0 conformity but also does not result in any strain when purely rigid body displacements and rotations are specified as nodal parameters.

With (25a–c), (26a, b) and (29a, b), the frame function $\tilde{\mathbf{u}} = \{\tilde{w}, \tilde{\Theta}_x, \tilde{\Theta}_y\}$ along a particular side of the element may be conveniently written in a matrix form as follows:

- if $\tilde{p} = 1$

$$\tilde{\mathbf{u}} = \tilde{N}_A \mathbf{d}_A + \tilde{N}_B \mathbf{d}_B \quad (31)$$

where

$$\tilde{N}_A = \begin{bmatrix} \tilde{N}_A & -\frac{1}{8} {}^1\tilde{N}_C \Delta x_{BA} & -\frac{1}{8} {}^1\tilde{N}_C \Delta y_{BA} \\ 0 & \tilde{N}_A & 0 \\ 0 & 0 & \tilde{N}_A \end{bmatrix} \quad (31a)$$

$$\tilde{N}_B = \begin{bmatrix} \tilde{N}_B & \frac{1}{8} {}^1\tilde{N}_C \Delta x_{BA} & \frac{1}{8} {}^1\tilde{N}_C \Delta y_{BA} \\ 0 & \tilde{N}_B & 0 \\ 0 & 0 & \tilde{N}_B \end{bmatrix} \quad (31b)$$

- if $\tilde{p} > 1$

$$\tilde{\mathbf{u}} = \tilde{N}_A \mathbf{d}_A + \tilde{N}_B \mathbf{d}_B + \tilde{N}_C \mathbf{d}_C = \tilde{N}_A \mathbf{d}_A + \tilde{N}_B \mathbf{d}_B + \sum_{i=1}^{\tilde{p}-1} {}^i\tilde{N}_C {}^i\mathbf{d}_C \quad (32)$$

where

$$\tilde{N}_A = \tilde{N}_A \mathbf{I}, \quad \tilde{N}_B = \tilde{N}_B \mathbf{I} \quad (32a, b)$$

\mathbf{I} is a 3×3 unit matrix

$${}^i\tilde{N}_C = {}^i\tilde{N}_C \mathbf{I} \quad (i = 1, 2, \dots, \tilde{p} - 2) \quad \text{to be used only if } \tilde{p} > 2! \quad (32c)$$

and

$${}^{\tilde{p}-1}\tilde{N}_C = \begin{bmatrix} {}^{\tilde{p}-1}\tilde{N}_C & \frac{\Delta x_{BA}}{2(1+\tilde{p})} {}^{\tilde{p}-1}\tilde{N}_C & \frac{\Delta y_{BA}}{2(1+\tilde{p})} {}^{\tilde{p}-1}\tilde{N}_C \\ 0 & {}^{\tilde{p}-1}\tilde{N}_C & 0 \\ 0 & 0 & {}^{\tilde{p}-1}\tilde{N}_C \end{bmatrix} \quad (32d)$$

2.5. Implementation of the new family of HT elements

The element will be designated according to the scheme

$$\tilde{\mathbf{Q}}\text{ab-c/d} \quad (33a)$$

where (see Sections 2.3 and 2.4), $a = \tilde{p} + 1$ is the order of boundary approximation for \tilde{w} , $b = \tilde{p}$ is the order of boundary approximation for $\tilde{\Theta}_x$ and $\tilde{\Theta}_y$, c is the number of functions in the polynomial—set (22a), and d is the number of functions in the set of modified Bessel functions (22b).

A simplified designation

$$\tilde{\mathbf{Q}}\text{ab-c rather than } \tilde{\mathbf{Q}}\text{ab-c/0} \quad (33b)$$

will be used if set (22b) is missing. A similar designation, namely $\mathbf{Q}\text{ab-c}$, has been used in [14]. The tilde over \mathbf{Q} (quadrilateral) in (33a, b) has been added in order to allow the present and the Petrolito elements [14] to be distinguished.

As for all HT elements (see e.g. [6–14]), the necessary (but not sufficient) condition for the resulting stiffness matrix (9b) to have full rank may be stated as

$$m \geq \text{NDOF} - \text{NRIG} = \text{NDOF} - 3 \tag{34}$$

where m is the number of homogeneous solutions, N_i , in the internal field (6), NDOF is the number of element degrees of freedom (field (7)), and NRIG is the number of rigid body modes (NRIG = 3 for plate bending). Though using the minimum number of N_i functions from (34) does not always guarantee an element with full rank, full rank can always be achieved by including more N_i functions into the internal field (6). In the present case the situation is considerably complicated owing to the fact that the same m may be obtained by a large number of combinations of the numbers of functions taken from either of the independent sets (22a) and (22b). The \tilde{Q} ab-c/d elements displayed in Table 2 are consistent with the scheme of alternating the (22a) and (22b) functions, as shown in Table 1. They have been numerically tested and found to exhibit no rank deficiency and to perform better than other possible combinations of the (22a) and (22b) functions. The \tilde{Q} ab-c elements with purely polynomial functions (22a) have also been considered. Though some of them (\tilde{Q} 21-11 and \tilde{Q} 43-33) exhibit one spurious zero energy mode, they may still be considered as practically robust since this mode is not commutable in most practical situations (see Table 2) provided that the plate has at least a minimal support (3DOF blocked so as to prevent rigid body modes). Indeed, in such cases global singularity does not occur and such elements may be largely preferable to formally flawless (no spurious zero energy mode) but practically too rigid \tilde{Q} 21-17 and \tilde{Q} 43-41 elements.

In addition to the above, the following two points must be noted when implementing the present family of elements:

- (1) To prevent matrix H from being singular, polynomial set (20) does not include the rigid body modes. As a consequence, internal displacement field (6) will be in error by rigid body components [6, 7]. If displacements inside the element are required, then field (6) has to be augmented with three rigid body modes (index r)

$$u_r = \begin{bmatrix} 1 & x & y \\ 0 & 1 & 0 \\ 0 & 0 & 1 \end{bmatrix} \begin{Bmatrix} c_{1r} \\ c_{2r} \\ c_{3r} \end{Bmatrix} \tag{35}$$

where c_{1r} , c_{2r} and c_{3r} are undetermined coefficients to be calculated by a simple procedure [6, 7] used to make the augmented internal field to match in a least-square sense the independent displacement frame \tilde{u} of the element. A simple, but less accurate alternative (not used here) consists in calculating the displacements from the auxiliary field \tilde{u} , which in the present case (C^0

Table 2

Overview of new HT quadrilateral thick plate elements with either T-complete (polynomials + modified Bessel) or incomplete (purely polynomial) sets of Trefftz function

M	Number of DOF	Condition (34)	Element	Actual m	Spurious modes	Min m for full rank
0	12	$m \geq 9$	\tilde{Q} 21-9/1	10	0	–
			\tilde{Q} 21-11	11	1Na	17
3	24	$m \geq 21$	\tilde{Q} 32-17/5	22	0	–
			\tilde{Q} 32-21	21	0	–
6	36	$m \geq 33$	\tilde{Q} 43-25/9	34	0	–
			\tilde{Q} 43-33	33	1Nb	41
9	48	$m \geq 45$	\tilde{Q} 54-33/13	46	0	–
			\tilde{Q} 54-45	45	0	–

Na—non-commutable in a mesh of 2 or more elements.

Nv—non-commutable with a minimum of 2×2 elements.

conformity) may easily be defined over the element area rather than only at the boundary of the element.

- (2) To ensure good numerical conditioning of matrix \mathbf{H} , the local coordinates x and y originated at the element center (Fig. 2) should be scaled, e.g. dividing them by the average distance between the origin and the element corners.

3. Assessment

3.1. Preliminary remarks

Unlike the classical thin plate theory, the Reissner–Mindlin theory requires three independent boundary conditions to be prescribed at the boundary of the plate, namely:

- $w = M_n = M_{nt} = 0$. . . soft simple support (SS1)
- $w = M_n = \Theta_t = 0$. . . hard simple support (SS2)
- $w = \Theta_n = \Theta_t = 0$. . . clamped edge (C)
- $Q_n = M_n = M_{nt} = 0$. . . free edge (F)

Most of the numerical studies presented in this section refer to the conventionally used square plate test (Fig. 3). Unless stated otherwise, the information about the mesh density concerns a symmetric quadrant of the plate. Furthermore, a Poisson ratio of $\nu = 0.3$ has been used in all examples and the displacement results are the frame values ($w = \tilde{w}$).

The converged reference results of the thick plate theory (results designated as ‘exact’ in the following studies) have been generated

- by application of the method outlined in the soft simple support (SS1) in [30]
- by series solution presented for the hard simple support (SS2) in [29]
- by application of the methods outlined, for the clamped edge (C) and for the combination of the free (F) and simply supported (SS2) boundaries (Fig. 3(d)), in [30]

Table 3 summarizes the reference results for different span to thickness ratios, L/h , used in subsequent studies.

3.2. Uniformly loaded square plate with hard simple support (SS2)

3.2.1. h - and p -convergence study with purely polynomial T -function

The aim of this study was to investigate the performance of the \tilde{Q}_{ab-c} elements from Table 4. The results for the central displacement and bending moment for a thick plate ($L/h = 10$), a thin plate ($L/h = 100$) and a very thin plate ($L/h = 1000$) are given in Table 4. It can be seen that both the h - and the p -extensions perform very nicely and that no shear locking appears for the thinnest plate with $L/h = 1000$. In this case the thick plate theory approximates well the classical thin plate solution,

$$Dw_C = 0.00406235\bar{p}L^4, \quad M_{x_C} = 0.0478864\bar{p}L^2,$$

obtained from the converged double series Navier solution [29].

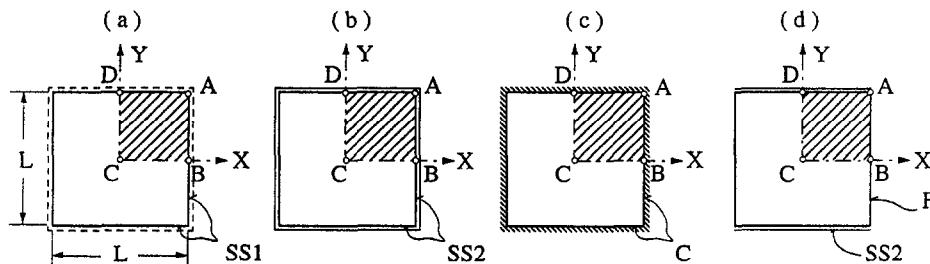


Fig. 3. Benchmark examples of square plates with various boundary conditions. SS1—soft simple support, SS2—hard simple support, C—clamped edge, F—free edge. Hatched area—discretized symmetric plate quadrant (unless stated otherwise, the mesh density indication given in the text concerns this quadrant).

Table 3
Reference results for uniformly loaded square plate ($\nu = 0.3$)

Boundary conditions	Quantity	$L/h = 10$	$L/h = 40$	$L/h = 100$	$L/h = 1000$
SS1 Fig. 3(a)	$10^2 D w_C : p L^4$	0.461691	0.416283		
	$10 M_{x,C} : p L^2$	0.509571	0.486616		
	$Q_{x,B} : p L$	-0.421434	-0.420835		
SS2 Fig. 3(b)	$10^2 D w_C : p L^4$	0.427284	0.407551	0.406446	0.406237
	$10 M_{x,C} : p L^2$	0.478864	0.478864	0.478864	0.478864
	$Q_{x,B} : p L$	-0.337660	-0.337660	-0.337660	-0.337660
C Fig. 3(c)	$10^2 D w_C : p L^4$	0.15046	0.12811		
	$10 M_{x,C} : p L^2$	0.23200	0.22931		
	$10 M_{x,B} : p L^2$	-0.49370	-0.51192		
	$Q_{x,B} : p L$	-0.41219	-0.43572		
F + SS2 Fig. 3(d)	$10^2 D w_B : p L^4$	0.156001	0.15091		
	$10 M_{x,C} : p L^2$	0.256394	0.26760		
	$10 M_{y,B} : p L^2$	-0.127605	-0.13021		
	$Q_{y,D} : p L$	-0.464970	-0.46776		

Table 4

Central deflection and central moment for simply supported (SS2) square plate (Fig. 3(b)) solved with $\tilde{Q}ab-c$ type of thick plate elements. h - and p -convergence study for $L/h = 10, 100$ and 1000

Mesh over sym. quadrant	M	$L/h = 10$		$L/h = 100$		$L/h = 1000$	
		$10^2 D w : \bar{p} L^4$	$10 M_x : \bar{p} L^2$	$10^2 D w : \bar{p} L^4$	$10 M_x : \bar{p} L^2$	$10^2 D w : \bar{p} L^4$	$10 M_x : \bar{p} L^2$
1×1	0	0.418754	0.487982	0.390909	0.474130	0.390628	0.473960
	3	0.426476	0.482045	0.405531	0.489321	0.405318	0.489454
	6	0.427448	0.479180	0.406596	0.478509	0.406388	0.478492
	9	0.427284	0.478895	0.406440	0.478811	0.406231	0.478796
2×2	0	0.428157	0.480086	0.405878	0.478462	0.405650	0.478419
	3	0.427241	0.478658	0.406410	0.479022	0.406202	0.479029
	6	0.427288	0.478870	0.406447	0.478830	0.406239	0.478832
	9	0.427284	0.478864	0.406446	0.478865	0.406237	0.478865
4×4	0	0.427644	0.479043	0.406510	0.478868	0.406296	0.478856
	3	0.427282	0.478835	0.406444	0.478877	0.406236	0.478879
	6	0.427284	0.478866	0.406446	0.478861	0.406237	0.478861
	9		0.478864		0.478864		0.478864
8×8	0	0.427379	0.478877	0.406474	0.478866	0.406265	0.478864
	3	0.427284	0.478862	0.406446	0.478864	0.406237	
	6		0.478864				
	9						
Exact		0.427284	0.478864	0.406446	0.478864	0.406237	0.478864

3.2.2. Comparison of the ‘new’ frame with ‘old’ frame elements [14]

The aim of this section is to study the consequences of replacing in Petrolito’s elements [14] the old definition (26c), of \tilde{w} by the new one (29a, b). The definitions (26a, b) of the rotations $\tilde{\theta}_x, \tilde{\theta}_y$ as well as that of the purely polynomial set of initial Trefftz functions defined by (22a) and (20), remain unchanged. Table 5 shows an overview of the ‘old frame’ and the ‘new frame’ elements involved in this

Table 5

HT elements with polynomial Trefftz functions. Overview of 'old frame' elements of [14] and present 'new frame' elements

M	0	1	3	4	6	9		
NDOF	12	16	24	28	36	48		
Element Formulation	$\tilde{Q}21-11$ Present	Q21-15S [14]	Q22-21 [14]	$\tilde{Q}32-21$ Present	Q32-25 [14]	Q33-33 [14]	$\tilde{Q}43-33$ Present	$\tilde{Q}54-45$ Present
Number and type of spurious modes	1Na	0	0	0	3Nb	2Na	1Nb	0
Min. m for full rank	17	–	–	–	33	35	41	–

Na—non-commutable with a mesh of 2 or more elements.

Nb—non-commutable with a minimum of 2×2 elements.

study. Here, the element Q21-15S of [14] has been obtained by using the first 13 Trefftz terms plus terms 16 and 17 from the generating sequence (20). As stated earlier, the advantage of the new definition of \tilde{w} over the old one is the fact that, with equal number M of side modes DOF, the polynomial representing the new \tilde{w} is one degree higher than that of the old one.

The results in Table 6 (for $L/h = 10$) and Table 7 (for $L/h = 1000$) are presented in the form of the percentage errors defined as

$$\Delta f \% = \frac{f_{FE} - f_{EX}}{f_{EX}} \times 100, \quad (36)$$

where f stands in turn for w_C , M_{x_C} and Q_{x_B} and where f_{FE} and f_{EX} are respectively, the finite element results and the converged reference results from Table 3. Whenever available, the 'old frame' results have been taken from [14]. Moreover, in order to complete some missing 'old frame' results, the family of Petrolito's elements has also been implemented into the FE library of the FE program SAFE [31]. The percentage errors in Tables 6 and 7 correspond to the frame values $w_C = \tilde{w}_C$ for displacements and to values derived from the internal Trefftz field (1) for M_{x_C} and Q_{x_B} . Unlike [14], no smoothing technique, such as, e.g. in [32–35], has been applied here to improve the predicted results for transverse shear forces.

Table 6

Comparison of 'old frame' ([14]) and 'new frame' HT elements from Table 5. % errors in w_C , M_{x_C} and Q_{x_B} for simply supported (SS2) uniformly loaded square plate (Fig. 3(b)). $L/h = 10$ (thick plate)

% error	Mesh	$M = 0$	$M = 1$	$M = 3$		$M = 4$	$M = 6$		$M = 9$
		Present	Ref. [14]	Ref. [14]	Present	Ref. [14]	Ref. [14]	Present	Present
Δw_C %	1×1	-1.996	-2.233	0.435	-0.187	-0.117	-0.220	0.040	0.000
	2×2	0.204	-0.102	-0.021	-0.009	-0.002	-0.007	0.002	
	4×4	0.084	-0.013	-0.003	0.000	0.000	0.000	0.000	
	8×8	0.022	0.006	0.000					
	16×16	0.011	0.001						
ΔM_{x_C} %	1×1	1.905	6.294	11.066	0.664	-0.581	-3.517	0.067	0.008
	2×2	0.257	1.485	1.380	-0.042	-0.002	-0.136	0.006	0.000
	4×4	-0.038	0.111	0.100	-0.004	0.002	-0.006	0.002	
	8×8	-0.004	0.008	0.006	0.000	0.000	0.000	0.000	
	16×16	0.000	0.002	0.002					
ΔQ_{x_B} %	1×1	-22.537	-43.834	23.275	-2.544	-8.446	19.606	-2.346	0.311
	2×2	-13.289	-4.519	29.468	-2.218	-0.829	5.245	-0.193	0.006
	4×4	-7.590	-0.811	13.564	-0.681	-0.175	0.924	-0.018	
	8×8	-4.176	-0.124	4.351	-0.160	-0.033	0.133	-0.003	
	16×16	-2.197	-0.021	1.211	-0.036	-0.006	0.018	0.000	

Table 7

Comparison of ‘old frame’ ([14]) and ‘new frame’ HT elements from Table 5. % errors in w_C , M_{x_C} and Q_{x_B} for simply supported (SS2) uniformly loaded square plate (Fig. 3(b)). $L/h = 1000$

% error	Mesh	$M = 0$	$M = 1$	$M = 3$		$M = 4$	$M = 6$		$M = 9$
		Present	Ref. [14]	Ref. [14]	Present	Ref. [14]	Ref. [14]	Present	Present
Δw_C %	1×1	-3.84	-4.10	-1.65	-0.23	-0.12	-0.08	0.04	-0.00
	2×2	-0.14	-1.02	-0.62	-0.01	-0.00	0.01	0.00	
	4×4	0.02	-0.26	-0.16	-0.00		0.00		
	8×8	0.01	-0.06	-0.04					
	16×16	0.00	-0.02	-0.01					
ΔM_{x_C} %	1×1	-1.02	12.46	28.30	2.21	-1.87	-11.30	-0.08	-0.01
	2×2	-0.09	6.96	6.15	0.03	-0.01	-1.73	-0.01	0.00
	4×4	0.00	1.65	1.50	0.00	-0.00	-0.31	-0.00	
	8×8		0.40	0.37			-0.07		
	16×16		0.10	0.09			-0.02		
ΔQ_{x_B} %	1×1	-25.96	-70.64	66.58	0.73	-18.51	62.44	0.97	-0.43
	2×2	-16.16	-12.86	159.32	-4.19	12.84	44.70	-1.53	-0.02
	4×4	-8.68	-6.24	216.51	-1.83	10.23	27.93	-0.14	0.00
	8×8	-4.49	-4.53	247.44	-1.05	-5.80	15.54	-0.02	
	16×16	-2.28	-2.69	260.04	-0.57	-0.75	7.94	-0.00	

Tables 6 and 7 shows that the ‘new frame’ results compare favorably with the ‘old frame’ solution. In addition to being more accurate in terms of the number of unknowns, they exhibit, as a rule, faster h - and p -convergence rates. It is also interesting to point out that, for a thin plate with $L/t = 1000$, the ‘old frame’ prediction of Q_{x_B} in Table 7 diverges for $M = 3$, whereas no such problem is encountered with the ‘new frame’ elements.

The comparison of the ‘old’ and the ‘new frame’ solutions for shear forces displayed in Figs. 4(a) and (b) completes the study.

3.2.3. Comparison of solutions with incomplete and T-complete Trefftz functions fields

The two families of p -elements of Table 2 have been applied in turn in order to compare their accuracy and their h - and p -convergence. The study of results and of percentage errors in displacements, moments and shear forces displayed on Tables 8 and 9, has led to the conclusion that in the case of hard simple support (SS2), the two families of elements yield a comparable degree of accuracy. However, from the computational point of view, the elements of the $\bar{Q}ab$ -c/d family are more expensive to generate owing to a slightly larger number of Trefftz functions (see Table 2) and a higher cost of numerical integration of the non-polynomial functions (22b).

3.2.4. Sensitivity to mesh distortion

This study is based on the comparison of percentage errors for the uniform and distorted 4×4 meshes over the whole plate (Fig. 5). Both the thick ($L/h = 10$) and very thin ($L/h = 1000$) plates have been considered, and their results have been displayed in Tables 10 and 11. As expected, this study has confirmed that the results are not too sensitive to mesh distortion. This feature, typical for all HT elements (see e.g. [1, 3, 5–7, 13, . . .]), is mainly due to the fact that the internal Trefftz field of each elements is defined in his local cartesian coordinate system and, as a consequence, does not depend on mesh distortion.

3.2.5. Comparison with conventional isoparametric quadratic elements

Since its first publication in 1970, the Ahmad isoparametric quadratic element [36] has remained the most popular element for analysis of moderately thick plates with transverse shear deformation. The

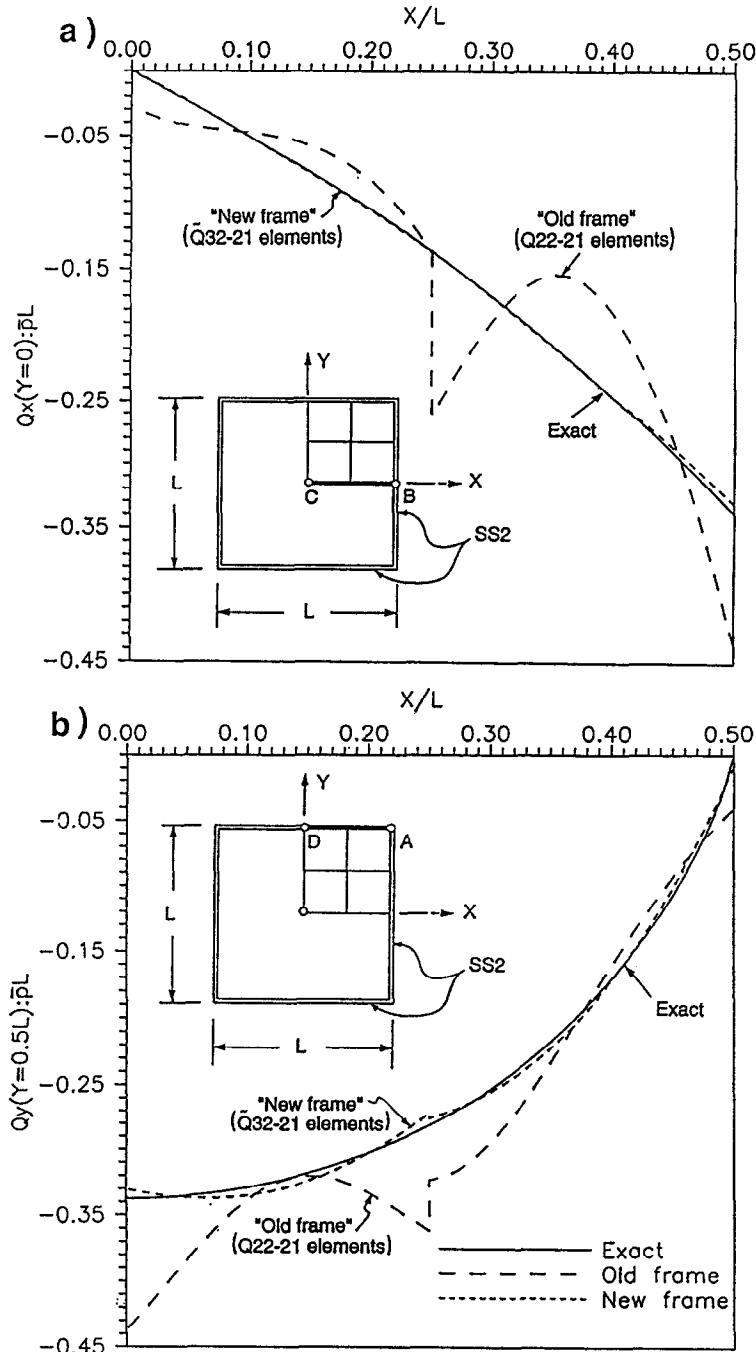


Fig. 4. Uniformly loaded simply supported (SS2) thick square plate ($L/h = 10$). Comparison of shear forces obtained with 2×2 mesh of 'old frame' (Q21-21) and 'new frame' (Q32-21) HT elements.

beneficial effect of the reduced 2×2 Gaussian points integration on attenuation of numerical difficulties encountered in the application of this element (further designated as CIQ) to thin plates, and known as 'shear locking', is now largely known and well understood [37]. Furthermore, the 'local smoothing' introduced by Hinton and Campbell [38]—a smoothing consisting of a bilinear extrapolation of results evaluated in the 2×2 Gauss points to the element nodes and of their subsequent averaging at nodes common to several elements—has been shown to be the simplest technique of sampling the solution results predicted by these elements.

Exactly as in the case of the CIQ elements, the Q32-31 and Q32-17/5 members of the two families of

Table 8

Uniformly loaded simply supported (SS2) thick square plate ($L/h = 10$). Comparison of solutions with incomplete (\tilde{Q}_{ab-c}) and T-complete ($\tilde{Q}_{ab-c/d}$) Trefftz function sets

Quantity	Mesh	$M = 0$		$M = 3$		$M = 6$		$M = 9$		Exact
		\tilde{Q}_{21-11}	$\tilde{Q}_{21-9/1}$	\tilde{Q}_{32-21}	$\tilde{Q}_{32-17/5}$	\tilde{Q}_{43-33}	$\tilde{Q}_{43-25/9}$	\tilde{Q}_{54-45}	$\tilde{Q}_{54-33/13}$	
$10^3 \frac{Dw_c}{\bar{p}L^4}$	1 × 1	4.1875	4.1875	4.2648	4.2708	4.2746	4.2752	4.2728	4.2729	4.27284
	2 × 2	4.2816	4.2818	4.2724	4.2723	4.2729	4.2729	4.2728	4.2728	
	4 × 4	4.2764	4.2765	4.2728	4.2728	4.2728	4.2728			
	8 × 8	4.2738	4.2738							
	16 × 16	4.2738	4.2731							
$10^2 \frac{M_{xc}}{\bar{p}L^2}$	1 × 1	4.8798	4.8798	4.8204	4.8947	4.7918	4.7892	4.7890	4.7934	4.78864
	2 × 2	4.8009	4.7987	4.7866	4.7866	4.7889	4.7874	4.7886	4.7886	
	4 × 4	4.7904	4.7906	4.7884	4.7882	4.7887	4.7886			
	8 × 8	4.7888	4.7888	4.7886	4.7886	4.7886	4.7886			
	16 × 16	4.7886	4.7887							
$10 \frac{Q_{xB}}{\bar{p}L}$	1 × 1	-2.6156	-2.6156	-3.2907	-3.2560	-3.2974	-3.6227	-3.3871	-3.3323	-3.3766
	2 × 2	-2.9279	-3.0583	-3.3017	-3.2862	-3.3701	-3.3867	-3.3768	-3.3764	
	4 × 4	-3.1203	-3.1314	-3.3536	-3.3552	-3.3760	-3.3768	-3.3766	-3.3766	
	8 × 8	-3.2356	-3.2362	-3.3712	-3.3732	-3.3765	-3.3766			
	16 × 16	-3.3024	-3.3024	-3.3754	-3.3762	-3.3766	-3.3766			

Table 9

Uniformly loaded simply supported (SS2) thick square plate ($L/h = 10$). % errors of solutions with incomplete (\tilde{Q}_{ab-c}) and T-complete ($\tilde{Q}_{ab-c/d}$) expansion sets

Quantity	Mesh	$M = 0$		$M = 3$		$M = 6$		$M = 9$	
		\tilde{Q}_{21-11}	$\tilde{Q}_{21-9/1}$	\tilde{Q}_{32-21}	$\tilde{Q}_{32-17/5}$	\tilde{Q}_{43-33}	$\tilde{Q}_{43-25/9}$	\tilde{Q}_{54-45}	$\tilde{Q}_{54-33/13}$
$\Delta w_c \%$	1 × 1	-2.00	-2.00	-0.19	-0.05	0.04	0.06	-0.00	0.00
	2 × 2	0.21	0.21	-0.01	-0.01	0.00	0.00		
	4 × 4	0.08	0.09	0.00	0.00				
	8 × 8	0.02	0.02						
	16 × 16	0.02	0.01						
$\Delta M_{xc} \%$	1 × 1	1.90	1.90	0.66	2.21	0.07	0.01	0.01	0.10
	2 × 2	0.26	0.21	-0.04	-0.04	0.01	-0.03	0.00	0.00
	4 × 4	0.04	0.04	-0.01	-0.01	0.00	0.00		
	8 × 8	0.00	0.00	0.00	0.00				
$\Delta Q_{xB} \%$	16 × 16								
	1 × 1	-22.53	-22.53	-2.54	-3.57	-2.35	7.29	0.31	-1.31
	2 × 2	-13.29	-9.41	-2.22	-2.68	-0.19	0.30	0.01	-0.01
	4 × 4	-7.59	-7.26	-0.68	-0.63	-0.02	0.01	0.00	0.00
	8 × 8	-4.18	-4.16	-0.16	-0.10	-0.00	0.00		
16 × 16	-2.20	-2.20	-0.04	-0.01					

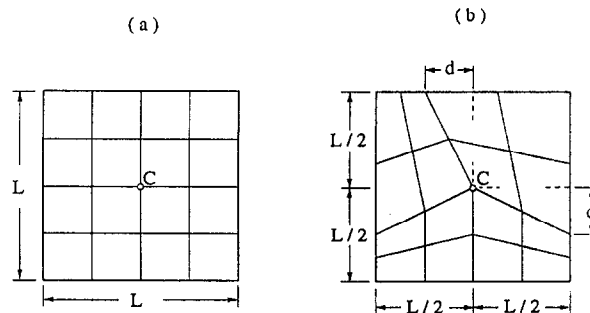


Fig. 5. Undistorted (a) and distorted (b) 4×4 meshes of quadrilateral HT thick plate elements.

Table 10

% errors for uniform (Fig. 5(a)) and distorted (Fig. 5(b)) 4 × 4 FE mesh. Uniformly loaded simply supported (SS2) thick square plate (L/h = 10)

M	Element type	ΔW_c %			ΔM_{xc} %		
		Uniform mesh	Distorted mesh		Uniform mesh	Distorted mesh	
			d = L/8	d = L/4		d = L/8	d = L/4
0	$\tilde{Q}21-11$	0.20	-0.13	-1.06	0.26	2.58	5.53
	$\tilde{Q}21-9/1$	0.21	-0.11	-0.97	0.21	-2.42	3.34
3	$\tilde{Q}32-21$	-0.01	-0.01	-0.01	-0.04	0.05	0.25
	$\tilde{Q}32-17/5$	-0.01	-0.01	-0.02	0.12	0.02	0.08
6	$\tilde{Q}43-33$	0.00	0.00	0.00	0.00	0.00	-0.01
	$\tilde{Q}43-25/9$	0.00	0.00	0.00	0.01	-0.00	-0.03
9	$\tilde{Q}54-45$	0.00	0.00	0.00	0.00	0.00	-0.00
	$\tilde{Q}54-33/13$	0.00	0.00	0.00	0.01	-0.00	0.00
Exact		$w_c = 0.00427284\bar{p}L^4/D$			$M_{xc} = 0.0478864\bar{p}L^2$		

Table 11

% errors for uniform (Fig. 5(a)) and distorted (Fig. 5(b)) 4 × 4 FE mesh. Uniformly loaded simply supported (SS2) thick square plate (L/h = 1000)

M	Element type	ΔW_c %			ΔM_{xc} %		
		Uniform mesh	Distorted mesh		Uniform mesh	Distorted mesh	
			d = L/8	d = L/4		d = L/8	d = L/4
0	$\tilde{Q}21-11$	-0.14	-0.65	-2.10	-0.09	1.78	3.00
3	$\tilde{Q}32-21$	-0.01	-0.01	-0.02	0.03	0.08	-0.09
6	$\tilde{Q}43-33$	0.00	0.00	0.00	-0.01	-0.01	0.01
9	$\tilde{Q}54-45$	0.00	0.00	0.00	0.00	-0.00	0.01
Exact		$w_c = 0.00406237\bar{p}L^4/D$			$M_{xc} = 0.0478864\bar{p}L^2$		

the HT plate elements of Table 2, are 8 noded quadrilateral elements with a total of 24 DOF. It is therefore of particular interest to compare their performance with that of the CIQ elements. The results of this study are summarized in Tables 12 and 13 which show the percentage errors in displacements, bending moments and shear forces for a thick (L/h = 10) and thin (L/h = 1000) plate as a function of density of the FE mesh. It may be seen that the errors exhibited by the present HT elements are mostly one to two orders of magnitude smaller than those exhibited by the conventional CIQ elements.

3.3. Uniformly loaded square plate with soft simple support (SS1)

3.3.1. Imposing of the SS1 boundary conditions in FE calculation

The difficulty of accurately imposing the SS1 boundary conditions ($w = M_n = M_{nt} = 0$) is due to the fact that the conditions $M_n = M_{nt} = 0$ allow fully unconstrained rotations $\tilde{\Theta}_x$ and $\tilde{\Theta}_y$, but the imposing to zero of the displacement parameters alone

$$\tilde{w}_A = \tilde{w}_B = 0 \quad \text{in (29a)} \tag{37a}$$

or

$$\tilde{w}_A = \tilde{w}_B = {}^1\Delta\tilde{w}_C = \dots = \tilde{p}^{-1}\Delta\tilde{w}_C = 0 \quad \text{in (29b)} \tag{37b}$$

is not sufficient for \tilde{w} along the side A – B to vanish. Following [20], the simple device of setting

$${}^1\tilde{N}_C = 0 \quad \text{in (29a)} \tag{38a}$$

Table 12

Comparison of two variants ($\tilde{Q}32-21$ and $\tilde{Q}32-17/5$) of HT 24 DOF quadrilateral elements with conventional isoparametric quadratic element (CIQ). Uniformly loaded simply supported (SS2) thick square plate ($L/h = 10$)

Mesh	Element type	Δw_c %	ΔM_{x_c} %	ΔQ_{x_B} %
1 × 1	CIQ	-4.959	39.98	-45.33
	$\tilde{Q}32-21$	-0.188	0.672	-2.54
	$\tilde{Q}32-17/5$	-0.047	2.216	-3.57
2 × 2	CIQ	-0.155	7.818	-45.33
	$\tilde{Q}32-21$	-0.010	-0.043	-2.22
	$\tilde{Q}32-17/5$	-0.013	-0.043	-2.68
4 × 4	CIQ	-0.003	1.824	-15.83
	$\tilde{Q}32-21$	0.000	-0.005	-0.68
	$\tilde{Q}32-17/5$	0.001	-0.009	-0.63
8 × 8	CIQ	0.000	0.446	-8.58
	$\tilde{Q}32-21$	0.000	-0.001	-0.16
	$\tilde{Q}32-17/5$	0.000	-0.001	-0.10
16 × 16	CIQ	0.000	0.112	-4.46
	$\tilde{Q}32-21$	0.000	0.000	-0.04
	$\tilde{Q}32-17/5$	0.000	0.000	-0.01

Table 13

Comparison of quadrilateral 24 DOF HT $\tilde{Q}32-31$ element with conventional isoparametric quadratic element (CIQ). Uniformly loaded simply supported (SS2) thick square plate ($L/h = 1000$)

Mesh	Element type	Δw_c %	ΔM_{x_c} %	ΔQ_{x_B} %
1 × 1	CIQ	-61.44	1.866	-48.91
	$\tilde{Q}32-21$	-0.266	2.211	0.74
2 × 2	CIQ	-54.06	-42.20	-29.72
	$\tilde{Q}32-21$	-0.009	0.034	-4.19
4 × 4	CIQ	-0.409	1.469	-15.71
	$\tilde{Q}32-21$	0.000	0.003	-1.83
8 × 8	CIQ	-0.002	0.446	-8.58
	$\tilde{Q}32-21$	0.000	0.000	-1.05
16 × 16	CIQ	0.000	0.112	-4.55
	$\tilde{Q}32-21$	0.000	0.000	-0.57

and similarly, in our case, of

$$\tilde{p}\tilde{N}_c = 0 \quad \text{in (29b)} \tag{38b}$$

removes the link between \tilde{w} and $\tilde{\Theta}_i = (\tilde{\Theta}_x \Delta x_{BA} + \tilde{\Theta}_y \Delta y_{BA})/L_{AB}$ and yields vanishing \tilde{w} along whole side $A - B$.

The price paid for this facility is, however, a non-standard FE coding since (38a, b) has to be imposed at the element level, in the element subroutine. In the case of the Q21-11 element ($M = 0$), separately studied in [15], it has been shown that condition (37a) alone still leads to excellent results and allows a fast convergence to the exact solution. Similarly, for higher-order elements ($M > 0$), the condition (38b) may be neglected and the SS1 condition approached, without a significant loss of accuracy (see Table 14), in either of the following two ways:

- (1) We let rotation $\tilde{\Theta}_i$ be completely unconstrained and, as a consequence, we tolerate in (29) a small parasitic displacement

$$\frac{1}{2(1 + \tilde{p})} \tilde{p}\tilde{N}_c (\tilde{p}^{-1} \Delta \tilde{\Theta}_{x_c} \Delta x_{BA} + \tilde{p}^{-1} \Delta \tilde{\Theta}_{y_c} \Delta y_{BA}) = \frac{1}{2(1 + \tilde{p})} \tilde{p}\tilde{N}_c \tilde{p}^{-1} \Delta \tilde{\Theta}_{i_c} L_{BA} \tag{39}$$

Table 14

Uniformly loaded simply supported (SS1) square plate ($L/h = 10$). Comparison of alternative methods of imposition of SS1 boundary conditions. A 4×4 mesh of $\tilde{Q}32-17/5$ elements over symmetric quadrant

Method of imposing	No linking $\tilde{p}\tilde{N}_C = 0$	Last DOF of $\tilde{\theta}_i$, left free	Last DOF of $\tilde{\theta}_i$, blocked
$10^3 \frac{Dw_c}{\bar{p}L^4}$	4.6211	4.6233	4.6098
Δw_c %	0.09	0.14	-0.15
$10^2 \frac{M_{x,c}}{\bar{p}L^2}$	5.0997	5.1010	5.0903
$\Delta M_{x,c}$ %	0.08	0.11	-0.11
$10 \frac{Q_{x,B}}{\bar{p}L}$	-3.9511	-3.9037	-4.0709
$\Delta Q_{x,B}$ %	-6.25	-7.37	-3.40

where $\tilde{p}^{-1} \Delta \tilde{\theta}_{i,c}$ is the last parameter of tangent rotation $\tilde{\theta}_i$.

- (2) In order to cancel the above parasitic displacement and to obtain $\tilde{w} = 0$ along $A - B$, we accept a partial constraint on $\tilde{\theta}_i$,

$$\tilde{p}^{-1} \Delta \tilde{\theta}_{i,c} = 0. \quad (40)$$

Though the difference in accuracy is generally small (see Table 14), this method has a small advantage over method (1) and therefore will be applied in numerical studies presented in the following section.

3.3.2. Comparison of solutions with p -elements based on incomplete and T -complete sets of Trefftz functions

As compared to plates with a SS2 support, an accurate FE solution for the SS1 support is far more difficult to reach owing to a very pronounced boundary layer effect. A typical example of such an effect is shown in Fig. 6. The twisting moments and shear forces shown in this figure have been obtained by the application of the so-called segmentation method [39].

The HT element results displayed for $L/h = 10$ in Table 15 and the percentage errors shown for $L/h = 10$ and $L/h = 40$ in Tables 16 and 17 lead to the following conclusions:

- The p -extension based on the $\tilde{Q}ab-c$ elements diverges. Therefore, in only the polynomial set of Trefftz functions is available, the best choice is the h -extension based on the $\tilde{Q}21-11$ lowest order element.
- Both the h - and p -extension rapidly converge toward the exact results if use is made of the $\tilde{Q}ab-c/d$ elements. Nevertheless, the necessary condition for the p -extension to converge is a certain minimal density of the HT elements mesh (e.g. 2×2 for $L/h = 10$ and 4×4 for $L/h = 40$).

The above minimal density requirement is easy to understand. Clearly, the boundary layer effect and the much simpler low gradient behaviour farther away from the boundary cannot be accurately represented within a single band of elements adjacent to the plate edge. Furthermore, the width of the boundary layer decreases with decreasing L/h ratio of the plate.

3.4. Remaining types of boundary conditions

3.4.1. Uniformly loaded square plate with clamped edges

The results for $L/h = 10$ and the percentage errors for $L/h = 10$ and $L/h = 1000$ are displayed in Tables 18–20. As expected, both the h - and p -extension processes based on the $\tilde{Q}ab-c/d$ elements with

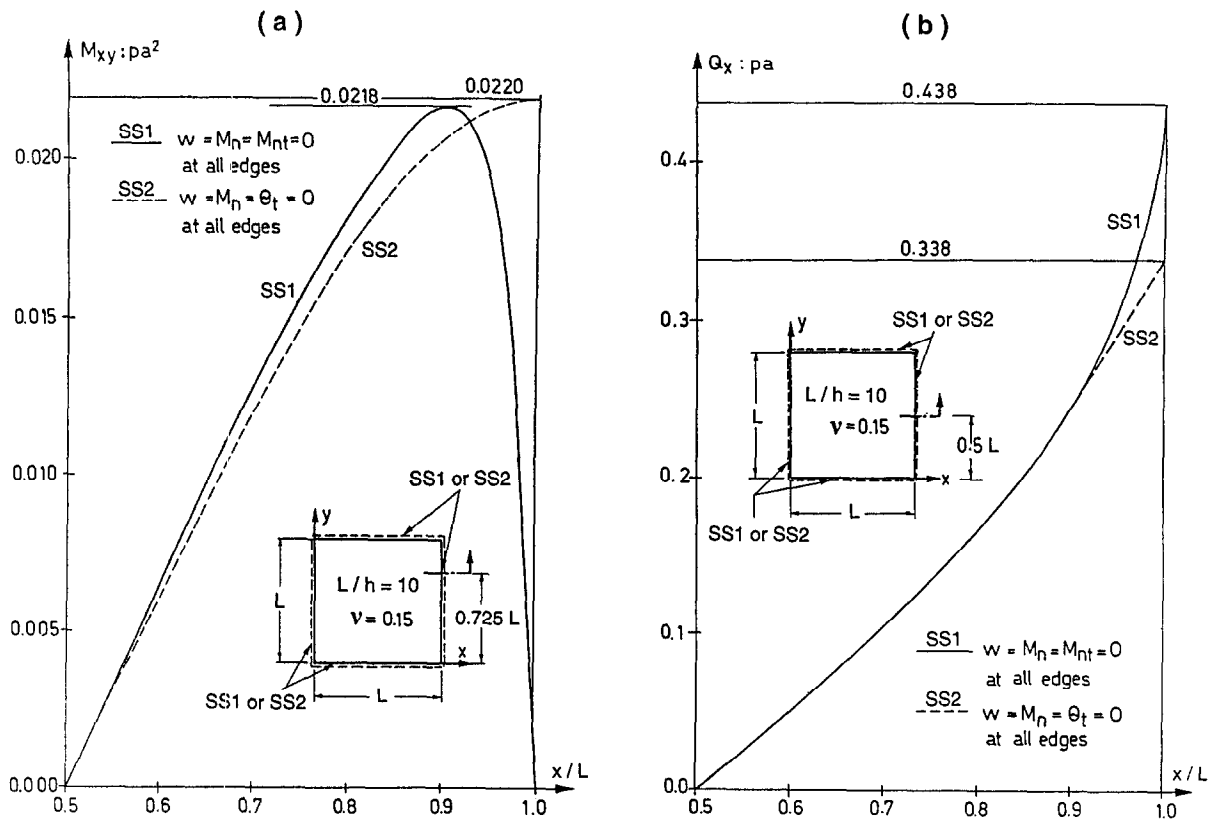


Fig. 6. Typical distributions of twisting moments (a) and shear forces (b) in uniformly loaded simply supported square plate.

Table 15

Uniformly loaded simply supported (SS1) thick square plate ($L/h = 10$). Comparison of solutions with incomplete (\tilde{Q}_{ab-c}) and T-complete ($\tilde{Q}_{ab-c/d}$) Trefftz functions sets

Quantity	Mesh	$M = 0$		$M = 3$		$M = 6$		$M = 9$		Exact
		\tilde{Q}_{21-11}	$\tilde{Q}_{21-9/1}$	\tilde{Q}_{32-21}	$\tilde{Q}_{32-17/5}$	\tilde{Q}_{43-33}	$\tilde{Q}_{43-25/9}$	\tilde{Q}_{54-45}	$\tilde{Q}_{54-33/13}$	
$10^3 \frac{Dw_c}{\bar{p}L^4}$	1 × 1	5.6689	4.6282	4.6223	4.5821	6.7896	4.7534	6.8876	4.6437	
	2 × 2	4.7122	4.5591	4.7235	4.5988	5.4271	4.6196	5.4643	4.6167	
	4 × 4	4.6184	4.5738	4.7133	4.6099	4.9563	4.6167	4.9854	4.6169	4.61691
	8 × 8	4.6183	4.5992	4.6602	4.6158	4.7403	4.6169	4.7652	4.6169	
	16 × 16	4.6151	4.6117	4.6303	4.6168	4.6529	4.6169	4.6618		
$10^2 \frac{M_{xc}}{\bar{p}L^2}$	1 × 1	7.2608	5.6160	4.9597	5.0277	6.5187	5.2415	6.4949	5.4652	
	2 × 2	4.8964	5.0626	5.2246	5.1272	5.8126	5.0845	5.8454	5.1004	
	4 × 4	5.0834	5.0584	5.1839	5.0896	5.3998	5.0955	5.4259	5.0957	5.09571
	8 × 8	5.0878	5.0794	5.1348	5.0948	5.2062	5.0957	5.2281	5.0957	
	16 × 16	5.0932	5.0909	5.1077	5.0956	5.1276	5.0957	5.1356		
$10 \frac{Q_{xB}}{\bar{p}L}$	1 × 1	-3.9991	-2.8822	-1.7602	0.9604	-0.9935	-4.6230	-2.3509	-6.0395	
	2 × 2	-3.4341	-2.6470	-2.6945	-3.1521	-3.0343	-4.5525	-2.7226	-4.1887	
	4 × 4	-3.6095	-3.8885	-3.7539	-4.0659	-3.4586	-4.2213	-2.6380	-4.2132	-4.21434
	8 × 8	-3.7295	-4.1046	-4.1186	-4.2042	-3.9417	-4.2116	-2.6246	-4.2182	
	16 × 16	-3.8794	-4.1825	-4.1983	-4.2178	-3.8163	-4.2168	-3.1733	-4.2184	

T-complete solution functions rapidly converge to the exact solution. In contrast, the \tilde{Q}_{ab-c} elements behave quite differently. While the h -extension converges again toward the exact results, this convergence is now slower than with $\tilde{Q}_{ab-c/d}$ elements. In the \tilde{Q}_{ab-c} case the mesh density, limited in Table 18 to 16×16 elements, had to be extended up to 64×64 elements, in order to confirm this

Table 16

Uniformly loaded simply supported (SS1) thick square plate ($L/h = 10$). % errors of solutions with incomplete (\tilde{Q}_{ab-c}) and T-complete ($\tilde{Q}_{ab-c/d}$) Trefftz functions sets

Quantity	Mesh	$M = 0$		$M = 3$		$M = 6$		$M = 9$	
		\tilde{Q}_{21-11}	$\tilde{Q}_{21-9/1}$	\tilde{Q}_{32-21}	$\tilde{Q}_{32-17/5}$	\tilde{Q}_{43-33}	$\tilde{Q}_{43-25/9}$	\tilde{Q}_{54-45}	$\tilde{Q}_{54-33/13}$
Δw_c %	1×1	22.79	0.24	0.15	-0.75	47.06	2.96	49.18	0.58
	2×2	2.06	-1.25	2.31	-0.39	17.55	0.06	18.35	-0.00
	4×4	0.03	-0.93	2.09	-0.15	7.35	-0.00	7.98	0.00
	8×8	0.03	-0.38	0.94	-0.02	2.67	0.00	3.21	
	16×16	-0.04	-0.11	0.29	-0.00	0.78		0.97	
$\Delta M_{x,c}$ %	1×1	42.49	10.21	-2.67	-1.33	27.93	2.86	27.46	7.25
	2×2	-3.91	-0.65	2.53	0.62	14.07	-0.22	14.72	0.09
	4×4	-0.24	-0.73	1.73	-0.12	5.97	-0.00	6.48	-0.00
	8×8	-0.16	-0.32	0.77	-0.02	2.17	-0.00	2.60	0.00
	16×16	-0.05	-0.09	0.24	-0.00	0.63		0.78	
$\Delta Q_{x,B}$ %	1×1	-5.11	-31.61	-58.23	-122.79	-76.43	9.70	-44.22	43.31
	2×2	-18.51	-37.19	-36.06	-25.21	-28.00	8.02	-35.40	-0.61
	4×4	-14.35	-7.73	-10.92	-3.52	-17.93	0.17	-37.40	-0.03
	8×8	-11.50	-2.60	-2.27	-0.24	-6.47	-0.07	-37.72	0.09
	16×16	-7.95	-0.76	-0.38	0.08	-9.44	0.06	-24.70	0.09

Table 17

Uniformly loaded simply supported (SS1) square plate ($L/h = 40$). % errors of solutions with incomplete (\tilde{Q}_{ab-c}) and T-complete ($\tilde{Q}_{ab-c/d}$) Trefftz functions sets

Quantity	Mesh	$M = 0$		$M = 3$		$M = 6$		$M = 9$	
		\tilde{Q}_{21-11}	$\tilde{Q}_{21-9/1}$	\tilde{Q}_{32-21}	$\tilde{Q}_{32-17/5}$	\tilde{Q}_{43-33}	$\tilde{Q}_{43-25/9}$	\tilde{Q}_{54-45}	$\tilde{Q}_{54-33/13}$
Δw_c %	1×1	27.49	27.49	3.40	3.02	57.12	53.21	60.15	35.17
	2×2	5.01	4.44	2.97	2.39	21.62	11.13	21.85	1.87
	4×4	1.14	0.66	1.74	0.57	9.07	0.50	9.16	0.01
	8×8	0.05	-0.32	1.12	-0.02	4.14	0.01	4.24	-0.00
	16×16	-0.12	-0.37	-0.70	-0.03	1.87	-0.00	2.00	-0.00
$\Delta M_{x,c}$ %	1×1	48.88	48.88	-1.42	8.42	35.09	37.21	35.56	-59.79
	2×2	-1.22	-0.28	2.85	1.14	16.26	7.79	16.46	2.20
	4×4	0.65	0.33	1.37	0.45	6.88	0.38	6.94	0.01
	8×8	0.01	-0.27	0.86	-0.02	3.15	0.01	3.22	-0.00
	16×16	-0.09	-0.29	-0.77	-0.02	1.42	-0.00	1.52	0.00
$\Delta Q_{x,B}$ %	1×1	-4.09	-4.09	-76.76	-171.66	-75.88	-232.46	-111.83	-166.95
	2×2	-16.86	-42.52	-61.19	-136.14	-15.50	282.60	-92.04	277.89
	4×4	-42.04	-80.65	-50.10	-98.46	-24.95	67.32	-57.43	21.04
	8×8	-10.79	-40.00	-29.85	-22.50	-24.81	8.02	-35.01	-0.69
	16×16	-10.16	-20.76	-19.24	-2.99	-16.09	0.17	-33.93	-0.02

statement. However, what is most interesting is the fact that for any fixed mesh density the p -extension now yields a different converged value. Though for practical purposes this fact is of little importance (whenever converged results were reached, their error with respect to the exact ones was only a fraction of percent), the difference is easily perceptible. Thus, e.g. the converged results for central deflection, as predicted by the \tilde{Q}_{54-45} elements in Table 18, are, respectively, equal to 1.5084, 1.5069, 1.5056 and 1.5050 for the meshes 2×2 , 4×4 , 8×8 and 16×16 , while the exact value is 1.5046 (as invariably obtained with the same meshes from the p -extension process based on the $\tilde{Q}_{ab-c/d}$ elements).

3.4.2. Uniformly loaded square plate with two edges free and two edges simply supported (Fig. 3(d))

The results for $L/h = 10$ and the percentage errors for $L/h = 10$ and $L/h = 40$ are displayed in Tables 21–23. Owing to the unconstrained tangent rotations along a part of the boundary, this example

Table 18

Uniformly loaded thick square plate ($L/h = 10$) with clamped boundaries. Comparison of solutions with incomplete (\tilde{Q}_{ab-c}) and T-complete ($\tilde{Q}_{ab-c/d}$) Trefftz functions sets

Quantity	Mesh	$M = 0$		$M = 3$		$M = 6$		$M = 9$		Exact
		\tilde{Q}_{21-11}	$\tilde{Q}_{21-9/1}$	\tilde{Q}_{32-21}	$\tilde{Q}_{32-17/5}$	\tilde{Q}_{43-33}	$\tilde{Q}_{43-25/9}$	\tilde{Q}_{54-45}	$\tilde{Q}_{54-33/13}$	
$10^2 \frac{Dw_B}{\bar{\rho}L^4}$	1 × 1	1.5634	1.5634	1.4882	1.4959	1.5131	1.5080	1.5106	1.5048	1.5046
	2 × 2	1.4801	1.4793	1.5072	1.5036	1.5084	1.5048	1.5084	1.5046	
	4 × 4	1.5012	1.5004	1.5066	1.5045	1.5069	1.5046	1.5069	1.5046	
	8 × 8	1.5039	1.5034	1.5056	1.5046	1.5056	1.5046	1.5056	1.5046	
	16 × 16	1.5044	1.5043	1.5049	1.5046	1.5050	1.5046	1.5050	1.5046	
$10^2 \frac{M_{xc}}{\bar{\rho}L^2}$	1 × 1	3.4722	3.4722	2.3723	2.5264	2.3336	2.3112	2.3378	2.2664	2.3200
	2 × 2	2.3323	2.3237	2.3154	2.3214	2.3246	2.3240	2.3238	2.3194	
	4 × 4	2.3278	2.3274	2.3214	2.3201	2.3222	2.3201	2.3222	2.3200	
	8 × 8	2.3214	2.3209	2.3209	2.3200	2.3210	2.3200	2.3210	2.3200	
	16 × 16	2.3203	2.3201	2.3203	2.3200	2.3203	2.3200	2.3203	2.3200	
$10 \frac{M_{yb}}{\bar{\rho}L^2}$	1 × 1	-4.3282	-4.3282	-4.9523	-5.6825	-4.7839	-5.1104	-4.8987	-4.7359	-4.9370
	2 × 2	-4.3485	-4.4771	-4.7552	-5.0814	-4.8855	-4.9614	-4.8989	-4.9197	
	4 × 4	-4.5516	-4.5750	-4.8607	-4.9574	-4.9140	-4.9428	-4.9134	-4.9355	
	8 × 8	-4.7272	-4.7322	-4.9120	-4.9398	-4.9279	-4.9380	-4.9267	-4.9369	
	16 × 16	-4.8284	-4.8294	-4.9298	-4.9374	-4.9340	-4.9371	-4.9336	-4.9370	
$10 \frac{Q_{yD}}{\bar{\rho}L}$	1 × 1	-3.4401	-3.4401	-4.4703	-5.8251	-4.2173	-4.3030	-4.2560	-3.7950	-4.1219
	2 × 2	-3.4447	-3.8340	-4.2143	-4.4136	-4.2668	-4.0889	-4.2165	-4.1134	
	4 × 4	-3.6970	-3.7993	-4.1723	-4.1448	-4.1945	-4.1234	-4.1740	-4.1219	
	8 × 8	-3.9027	-3.9366	-4.1433	-4.1216	-4.1495	-4.1233	-4.1432	-4.1219	
	16 × 16	-4.0197	-4.0312	-4.1286	-4.1215	-4.1303	-4.1222	-4.1285	-4.1219	

Table 19

Uniformly loaded thick square plate ($L/h = 10$) with clamped boundaries. % errors of solutions with incomplete (\tilde{Q}_{ab-c}) and T-complete ($\tilde{Q}_{ab-c/d}$) Trefftz functions sets

Quantity	Mesh	$M = 0$		$M = 3$		$M = 6$		$M = 9$	
		\tilde{Q}_{21-11}	$\tilde{Q}_{21-9/1}$	\tilde{Q}_{32-21}	$\tilde{Q}_{32-17/5}$	\tilde{Q}_{43-33}	$\tilde{Q}_{43-25/9}$	\tilde{Q}_{54-45}	$\tilde{Q}_{54-33/13}$
$\Delta w_c \%$	1 × 1	3.91	3.91	-1.09	-0.58	0.56	0.23	0.40	0.01
	2 × 2	-1.63	-1.68	0.17	-0.07	0.25	0.01	0.25	0.00
	4 × 4	-0.23	-0.28	0.13	-0.01	0.15	0.00	0.15	
	8 × 8	-0.05	-0.08	0.07	0.00	0.07		0.07	
	16 × 16	-0.01	-0.02	0.02		0.03		0.03	
$\Delta M_{xc} \%$	1 × 1	49.66	49.66	2.25	8.90	0.59	-0.38	0.77	-2.31
	2 × 2	0.53	0.16	-0.20	0.06	0.20	0.17	0.16	-0.03
	4 × 4	0.34	0.32	0.06	0.00	0.09	0.00	0.09	0.00
	8 × 8	0.06	0.04	0.04		0.04		0.04	
	16 × 16	0.01	0.00	0.01		0.01		0.01	
$\Delta M_{xb} \%$	1 × 1	-12.33	-12.33	0.31	15.10	-3.10	3.51	-0.78	-4.07
	2 × 2	-11.92	-9.32	-3.68	2.92	-1.04	0.49	-0.77	-0.35
	4 × 4	-7.81	-7.33	-1.55	0.41	-0.47	0.12	-0.48	-0.03
	8 × 8	-4.25	-4.15	-0.51	0.06	-0.18	0.02	-0.21	-0.00
	16 × 16	-2.20	-2.18	-0.15	0.01	-0.06	0.00	-0.07	
$\Delta Q_{xb} \%$	1 × 1	-16.54	-16.54	8.45	41.32	2.31	4.39	3.25	-7.93
	2 × 2	-16.43	-6.98	2.24	7.08	3.52	-0.80	2.30	-0.21
	4 × 4	-10.31	-7.83	1.22	0.56	1.76	0.04	1.26	0.00
	8 × 8	-5.32	-4.50	0.52	-0.01	0.67	0.03	0.52	
	16 × 16	-2.48	-2.20	0.16	-0.01	0.20	0.01	0.16	

Table 20

Uniformly loaded thick square plate ($L/h = 40$) with clamped boundaries. % errors of solutions with incomplete (\tilde{Q}_{ab-c}) and T-complete ($\tilde{Q}_{ab-c/d}$) Trefftz functions sets

Quantity	Mesh	$M = 0$		$M = 3$		$M = 6$		$M = 9$	
		\tilde{Q}_{21-11}	$\tilde{Q}_{21-9/1}$	\tilde{Q}_{32-21}	$\tilde{Q}_{32-17/5}$	\tilde{Q}_{43-33}	$\tilde{Q}_{43-25/9}$	\tilde{Q}_{54-45}	$\tilde{Q}_{54-33/13}$
Δw_c %	1 × 1	0.36	0.36	-1.63	-0.26	0.15	0.07	0.00	0.03
	2 × 2	-4.04	-4.03	-0.10	-0.08	0.01	0.01	0.00	0.00
	4 × 4	-0.88	-0.87	0.00	0.00	0.01	0.00	0.01	
	8 × 8	-0.18	-0.18	0.01		0.01		0.01	
	16 × 16	-0.04	-0.04	0.00		0.00		0.00	
ΔM_{xc} %	1 × 1	54.23	54.23	4.37	6.64	-0.47	-9.07	-0.06	1.27
	2 × 2	-3.68	-4.12	-0.06	0.07	-0.03	-0.35	0.01	0.00
	4 × 4	-0.05	0.03	0.00	0.02	0.00	-0.00	0.00	
	8 × 8	0.02	0.02		0.00				
	16 × 16	0.01	0.00						
ΔM_{xB} %	1 × 1	-12.36	-12.36	2.84	70.22	-3.19	6.60	-0.03	-0.10
	2 × 2	-10.05	-0.75	-3.56	13.36	-0.39	0.07	-0.05	-1.20
	4 × 4	-7.13	-6.51	-1.27	1.82	-0.08	0.12	-0.04	-0.22
	8 × 8	-4.19	-4.14	-0.36	0.21	-0.04	0.04	-0.03	-0.02
	16 × 16	-2.23	-2.21	-0.11	0.02	-0.02	0.01	-0.02	-0.00
ΔQ_{xB} %	1 × 1	-19.23	-19.23	10.17	670.68	-1.16	174.47	1.69	28.43
	2 × 2	-17.68	90.03	-0.38	149.37	1.60	7.26	0.75	-6.60
	4 × 4	-10.44	-1.91	0.53	21.28	1.64	-2.05	0.76	-1.59
	8 × 8	-5.95	-5.06	0.80	2.41	1.01	-0.25	0.61	-0.04
	16 × 16	-3.13	-2.66	0.46	0.14	0.48	0.01	0.34	0.00

Table 21

Uniformly loaded thick square plate ($L/h = 10$) with two sides free and two sides simply supported (Fig. 3(d)). Comparison of solutions with incomplete (\tilde{Q}_{ab-c}) and T-complete ($\tilde{Q}_{ab-c/d}$) Trefftz functions sets

Quantity	Mesh	$M = 0$		$M = 3$		$M = 6$		$M = 9$		Exact
		\tilde{Q}_{21-11}	$\tilde{Q}_{21-9/1}$	\tilde{Q}_{32-21}	$\tilde{Q}_{32-17/5}$	\tilde{Q}_{43-33}	$\tilde{Q}_{43-25/9}$	\tilde{Q}_{54-45}	$\tilde{Q}_{54-33/13}$	
$10^2 \frac{Dw_B}{\bar{p}L^4}$	1 × 1	1.7159	1.6491	1.6398	1.5804	2.2060	1.5632	2.9182	1.5607	
	2 × 2	1.5823	1.5732	1.5950	1.5622	1.6600	1.5598	1.7914	1.5600	
	4 × 4	1.5634	1.5594	1.5733	1.5601	1.5963	1.5600	1.6269	1.5600	1.56001
	8 × 8	1.5605	1.5588	1.5643	1.5600	1.5712	1.5600	1.5845	1.5600	
	16 × 16	1.5601	1.5596	1.5612	1.5600	1.5628	1.5600	1.5700	1.5600	
$10^2 \frac{M_{xc}}{\bar{p}L^2}$	1 × 1	1.4343	5.7816	2.6036	3.3280	2.2370	1.6064	1.2183	2.3008	
	2 × 2	2.6650	2.6833	2.2864	2.5959	2.0110	2.5673	1.6920	2.5624	
	4 × 4	2.5732	2.5950	2.4688	2.5669	2.3751	2.5640	2.2676	2.5639	2.56394
	8 × 8	2.5681	2.5772	2.5344	2.5642	2.5054	2.5639	2.4394	2.5639	
	16 × 16	2.5652	2.5680	2.5558	2.5640	2.5493	2.5639	2.5113	2.5639	
$10 \frac{M_{yB}}{\bar{p}L^2}$	1 × 1	1.3540	1.6860	1.6234	1.4662	1.3674	1.0337	0.7218	1.2349	
	2 × 2	1.3094	1.3498	1.3861	1.3037	1.3193	1.2504	0.7385	1.2806	
	4 × 4	1.2954	1.3062	1.3181	1.2785	1.3090	1.2752	0.9753	1.2769	1.27605
	8 × 8	1.2872	1.2907	1.2985	1.2764	1.2613	1.2762	1.1655	1.2761	
	16 × 16	1.2888	1.2835	1.2888	1.2762	1.2729	1.2761	1.2293	1.2760	
$10 \frac{Q_{yD}}{\bar{p}L}$	1 × 1	-3.1635	5.9682	-6.7957	-6.4079	-7.3974	-6.8432	-1.9047	-4.2774	
	2 × 2	-4.2438	-4.0143	-4.5763	-4.6418	-4.3890	-4.6674	-4.3613	-4.6417	
	4 × 4	-4.3549	-4.3452	-4.6154	-4.6372	-4.5915	-4.6496	-4.5581	-4.6497	-4.64970
	8 × 8	-4.4984	-4.5004	-4.6403	-4.6474	-4.6320	-4.6497	-4.6119	-4.6497	
	16 × 16	-4.5729	-4.5737	-4.6473	-4.6494	-4.6453	-4.6497	-4.6338	-4.6497	

Table 22

Uniformly loaded thick square plate ($L/h = 10$) with two sides free and two sides simply supported (Fig. 3(d)). % errors of solutions with incomplete (\tilde{Q}_{ab-c}) and T-complete ($\tilde{Q}_{ab-c/d}$) Trefftz functions sets

Quantity	Mesh	$M = 0$		$M = 3$		$M = 6$		$M = 9$	
		\tilde{Q}_{21-11}	$\tilde{Q}_{21-9/1}$	\tilde{Q}_{32-21}	$\tilde{Q}_{32-17/5}$	\tilde{Q}_{43-33}	$\tilde{Q}_{43-25/9}$	\tilde{Q}_{54-45}	$\tilde{Q}_{54-33/13}$
Δw_B %	1 × 1	9.99	5.71	5.11	1.31	41.41	0.20	87.06	0.04
	2 × 2	1.43	0.85	2.24	0.14	6.41	-0.01	14.83	0.00
	4 × 4	0.22	-0.04	0.85	0.01	2.33	0.00	4.29	
	8 × 8	0.03	-0.08	0.27	0.00	1.10		1.57	
	16 × 16	0.01	-0.03	0.08		0.18		0.64	
$\Delta M_{x,c}$ %	1 × 1	-44.06	125.50	1.55	29.80	-12.75	-37.35	-52.48	-10.26
	2 × 2	3.94	4.66	-10.82	1.25	-20.57	0.13	-34.01	-0.06
	4 × 4	0.36	1.21	-3.71	0.12	-7.37	0.00	-11.56	-0.00
	8 × 8	0.16	0.52	-1.15	0.01	-2.28	-0.00	-4.86	
	16 × 16	0.05	0.16	-0.32	0.00	-0.57		-2.05	
$\Delta M_{y,B}$ %	1 × 1	6.11	32.13	27.22	14.90	7.16	-18.99	-43.43	-3.22
	2 × 2	2.61	5.78	8.62	2.17	3.39	-2.01	-42.34	0.36
	4 × 4	1.52	2.36	3.30	0.19	2.58	-0.07	-23.57	0.07
	8 × 8	0.87	1.15	1.76	0.03	-1.16	0.01	-8.66	0.00
	16 × 16	1.00	0.58	1.00	0.01	-0.25	0.00	-3.66	
$\Delta Q_{y,D}$ %	1 × 1	-31.93	-228.36	46.15	37.81	59.09	47.18	-99.59	-8.01
	2 × 2	-8.73	-13.67	-1.58	-0.17	-5.61	0.38	-6.20	-0.17
	4 × 4	-6.34	-6.55	-0.74	-0.27	-1.25	-0.00	-1.97	0.00
	8 × 8	-3.23	-3.21	-0.20	-0.05	-0.38	0.00	-0.81	
	16 × 16	-1.65	-1.63	-0.05	-0.01	-0.09		-0.34	

Table 23

Uniformly loaded thick square plate ($L/h = 40$) with two sides free and two sides simply supported (Fig. 3(d)). % errors of solutions with incomplete (\tilde{Q}_{ab-c}) and T-complete ($\tilde{Q}_{ab-c/d}$) Trefftz functions sets

Quantity	Mesh	$M = 0$		$M = 3$		$M = 6$		$M = 9$	
		\tilde{Q}_{21-11}	$\tilde{Q}_{21-9/1}$	\tilde{Q}_{32-21}	$\tilde{Q}_{32-17/5}$	\tilde{Q}_{43-33}	$\tilde{Q}_{43-25/9}$	\tilde{Q}_{54-45}	$\tilde{Q}_{54-33/13}$
Δw_B %	1 × 1	11.01	7.11	3.26	3.71	29.13	23.86	80.93	18.02
	2 × 2	2.01	1.60	1.27	1.04	6.42	2.28	14.54	0.53
	4 × 4	0.47	0.32	0.68	0.24	2.59	0.09	4.47	0.01
	8 × 8	0.08	-0.01	0.39	0.03	1.09	0.00	1.48	0.00
	16 × 16	-0.00	-0.05	0.17	0.00	0.43		0.65	
$\Delta M_{x,c}$ %	1 × 1	-44.34	-31.31	-12.13	-30.09	-114.21	-153.33	-430.04	84.27
	2 × 2	0.93	11.04	-8.47	8.77	-20.08	-21.63	-32.85	-0.05
	4 × 4	-0.47	0.25	-2.97	0.56	-7.69	-0.28	-9.90	-0.01
	8 × 8	-0.02	0.24	-1.39	0.02	-3.22	-0.01	-4.00	0.00
	16 × 16	0.01	0.22	-0.57	0.00	-1.30	0.00	-1.89	
$\Delta M_{y,B}$ %	1 × 1	4.23	126.54	29.17	65.14	3.88	-123.48	-50.64	-237.09
	2 × 2	1.53	15.49	13.66	18.45	3.63	-36.20	-43.52	-21.36
	4 × 4	0.88	3.47	5.50	4.52	2.14	-4.58	-37.49	-0.47
	8 × 8	0.54	1.13	1.87	0.69	0.67	-0.44	-17.57	0.10
	16 × 16	0.32	0.51	0.75	0.08	0.05	0.16	-5.58	0.02
$\Delta Q_{y,D}$ %	1 × 1	-32.77	-415.42	66.24	1204.11	145.78	1964.14	-611.82	-4950.88
	2 × 2	-8.87	-141.08	-0.40	82.49	-3.19	132.00	-6.87	-9.95
	4 × 4	-6.17	-16.17	-1.47	2.35	-1.41	0.02	-1.77	0.01
	8 × 8	-3.29	-3.71	-0.53	-0.13	-0.56	0.00	-0.70	0.00
	16 × 16	-1.64	-1.63	-0.15	-0.07	-0.22		-0.33	

exhibits along the two free edges a strong boundary layer effect of a similar nature to that experienced in the case of the soft simple support, SS1, in Section 3.3.2. It is therefore not surprising that the properties of the \tilde{Q}_{ab-c} and $\tilde{Q}_{ab-c/d}$ solutions, as reported for the soft simple support, also apply to the present case. Indeed, the p -extension process based on the $\tilde{Q}_{ab-c/d}$ T-complete set elements converges toward the exact solution provided that the FE mesh has a certain minimum density (1×1 for $L/h = 10$ and 4×4 for $L/h = 40$ in the present case). Furthermore, the h -extension process with either of the two element types converges toward the exact solution and once more, if the \tilde{Q}_{ab-c} elements are used, the simplest of them, the \tilde{Q}_{21-11} element, yields the best results.

4. Concluding remarks

The basic contributions of the reported research on HT thick plate elements are:

- the implementation of a new type of the auxiliary frame field where the interpolation of the displacement \tilde{w} has been linked with that of the tangent rotation $\tilde{\Theta}_i$;
- the development of a T-complete set of Trefftz functions for representation of the internal displacements and rotations fields of the element.

As compared with the customary independent interpolations of displacements \tilde{w} and rotations $\tilde{\Theta}_x, \tilde{\Theta}_y$ [14], the main advantage of the new frame field is that the polynomial degree of \tilde{w} and the accuracy of the solution have been increased without augmenting either the number of DOF or the number of Trefftz functions of the element.

The main importance of the T-complete set of Trefftz functions (whereby the Petrolito's polynomial functions have been completed by additional modified Bessel functions) resides, however, in the fact that their application is necessary for warranting the convergence of the p -extension process toward the exact solution.

The element subroutine of the reported new elements in the FE program SAFE [31] enables one to choose either of the two alternative Trefftz functions sets and thus generate both the \tilde{Q}_{ab-c} and the $\tilde{Q}_{ab-c/d}$ elements. Based on extensive numerical studies (of which a part has been presented in Section 3), the h - and p -method convergence properties of these two element types have been summarized in Table 24. Either of them exhibits a remarkable insensitivity to mesh distortion (since no mapping has been involved in the formulation). Both the p -extension process based on the $\tilde{Q}_{ab-c/d}$ element family and h -extension process based on either of two families converge to the exact solution of the Reissner–Mindlin theory and tend in the thin limit, without locking, to the exact results of the classical thin plate (Kirchhoff) theory.

The only drawback of the T-complete Trefftz functions set over the incomplete polynomial one is the computational effort associated with numerical integration of the expressions involving the modified

Table 24

Convergence properties of HT thick plate elements with incomplete (\tilde{Q}_{ab-c}) and T-complete ($\tilde{Q}_{ab-c/d}$) Trefftz functions

Convergence process	T-functions	Element designation	Convergence/Divergence			
			SS2	C	F	SS1
h -extension	polynomials	\tilde{Q}_{ab-c}				
	polynomials + modif. Bessel f.	$\tilde{Q}_{ab-c/d}$			1	
p -extension	polynomials	\tilde{Q}_{ab-c}	1	2	3	3
	polynomials + modif. Bessel f.	$\tilde{Q}_{ab-c/d}$			1	

1. Convergence toward exact solution.
2. Convergence toward a solution close to the exact one.
3. Divergence.

Bessel functions. However, this effort can considerably be reduced if one observed that—except for the band of elements adjacent to the boundary—the non-polynomial part of the T-complete set of Trefftz functions in all remaining elements is not activated. Indeed, whenever the coefficients *c* of these functions were evaluated (relation (11)), then those of them corresponding to the non-polynomial functions in the T-complete sets were found negligible or vanishing. As a consequence (Tables 25–28)

Table 25

Uniformly loaded simply supported (SS1) square plate ($L/h = 40$). Comparison of solutions obtained with different combinations of \tilde{Q}_{ab-c} and $\tilde{Q}_{ab-c/d}$ elements in 4×4 FE mesh over symmetric plate quadrant

Quantity	Elements adjacent to boundary	Remaining elements	$M = 3$	$M = 6$	$M = 9$	Exact
$10^3 Dw_c: \bar{p}L^4$	$\tilde{Q}_{ab-c/d}$		4.18637	4.18374	4.16336	
	$\tilde{Q}_{ab-c/d} \tilde{Q}_{ab-c}$		4.18640	4.18387	4.16337	4.16283
	\tilde{Q}_{ab-c}		4.23521	4.54037	4.54401	
$10^2 M_{xc}: \bar{p}L^2$	$\tilde{Q}_{ab-c/d}$		4.88813	4.88451	4.86664	
	$\tilde{Q}_{ab-c/d} \tilde{Q}_{ab-c}$		4.88787	4.88467	4.86662	4.86616
	\tilde{Q}_{ab-c}		4.93257	5.20101	5.20413	

Table 26

Uniformly loaded simply supported (SS1) square plate ($L/h = 40$). % errors obtained with different combinations of \tilde{Q}_{ab-c} and $\tilde{Q}_{ab-c/d}$ elements in 4×4 FE mesh over symmetric plate quadrant

Quantity	Elements adjacent to boundary	Remaining elements	$M = 3$	$M = 6$	$M = 9$
$\Delta w_c \%$	$\tilde{Q}_{ab-c/d}$		0.57	0.50	0.01
	$\tilde{Q}_{ab-c/d} \tilde{Q}_{ab-c}$		0.57	0.51	0.01
	\tilde{Q}_{ab-c}		1.74	9.07	9.16
$\Delta M_{xc} \%$	$\tilde{Q}_{ab-c/d}$		0.45	0.38	0.01
	$\tilde{Q}_{ab-c/d} \tilde{Q}_{ab-c}$		0.45	0.38	0.01
	\tilde{Q}_{ab-c}		1.36	6.88	6.95

Table 27

Uniformly loaded thick square plate ($L/h = 10$) with clamped edges. Comparison of solutions obtained with different combinations of \tilde{Q}_{ab-c} and $\tilde{Q}_{ab-c/d}$ elements in 4×4 FE mesh over symmetric plate quadrant

Quantity	Elements adjacent to boundary	Remaining elements	$M = 3$	$M = 6$	$M = 9$	Exact
$10^3 Dw_c: \bar{p}L^4$	$\tilde{Q}_{ab-c/d}$		1.5045	1.5046	1.5046	
	$\tilde{Q}_{ab-c/d} \tilde{Q}_{ab-c}$		1.5045	1.5046	1.5046	1.5046
	\tilde{Q}_{ab-c}		1.5066	1.5069	1.5069	
$10^2 M_{xc}: \bar{p}L^2$	$\tilde{Q}_{ab-c/d}$		2.3201	2.3201	2.3200	
	$\tilde{Q}_{ab-c/d} \tilde{Q}_{ab-c}$		2.3193	2.3200	2.3200	2.3200
	\tilde{Q}_{ab-c}		3.3214	2.3222	2.3222	
$10^2 M_{xB}: \bar{p}L^4$	$\tilde{Q}_{ab-c/d}$		-4.9574	-4.9428	-4.9355	
	$\tilde{Q}_{ab-c/d} \tilde{Q}_{ab-c}$		-4.9571	-4.9236	-4.9355	-4.9370
	\tilde{Q}_{ab-c}		-4.8607	-4.9140	-4.9134	

Table 28

Uniformly loaded thick square plate ($L/h = 10$) with clamped edges. % errors obtained with different combinations of \tilde{Q}_{ab-c} and $\tilde{Q}_{ab-c/d}$ elements in 4×4 FE mesh over symmetric plate quadrant

Quantity	Elements adjacent to boundary	Remaining elements	$M = 3$	$M = 6$	$M = 9$
Δw_c %	$\tilde{Q}_{ab-c/d}$		-0.01	0.00	0.00
	$\tilde{Q}_{ab-c/d} \tilde{Q}_{ab-c}$		-0.01	0.00	0.00
	\tilde{Q}_{ab-c}		0.13	0.15	0.15
ΔM_{xc} %	$\tilde{Q}_{ab-c/d}$		0.00	0.00	0.00
	$\tilde{Q}_{ab-c/d} \tilde{Q}_{ab-c}$		-0.03	0.00	0.00
	\tilde{Q}_{ab-c}		0.06	0.09	0.09
ΔM_{xb} %	$\tilde{Q}_{ab-c/d}$		0.41	0.12	-0.03
	$\tilde{Q}_{ab-c/d} \tilde{Q}_{ab-c}$		0.41	-0.27	-0.03
	\tilde{Q}_{ab-c}		-1.55	-0.47	-0.48

the use of the more expensive $\tilde{Q}_{ab-c/d}$ elements may be restricted, without any loss of accuracy, to those adjacent to plate edges with SS1, F or C boundary conditions.

A recent comparative study [13] of conventional and HT thin plates, plane elasticity and Poisson's equation h - and p -elements has clearly shown the superiority of these elements over the conventional ones. In the present paper, similar studies have been confined (Section 3.2.5) to a comparison of the isoparametric quadratic elements (CIQ) with the \tilde{Q}_{32-31} and $\tilde{Q}_{32-17/5}$ HT elements. All of these elements have the same external appearance and the same number, 24, of DOF. As shown in Tables 12 and 13, the use of the HT elements makes it possible to reduce the errors mostly by more than one or two orders of magnitude as compared with the CIQ elements solution. This comparison is, however, biased, since the CIQ results for moments and shear forces have been obtained by the application of the well-known technique of local smoothing [38], while no such improvement of accuracy has been applied to the HT element solution. Indeed, here the results have been evaluated directly from the internal Trefftz function field at element corners, points where the error is the largest, while the use of the special smoothing technique, as devised for HT p -elements in [40], would probably make it possible to decrease these errors by at least one order of magnitude. Such an improvement is possible due to the known tendency of the HT elements to concentrate the errors in a narrow band along the element boundary and leave inside the element a large zone of superconvergence with errors one or two orders of magnitude smaller than at the element corners.

The application of uniform meshes is uneconomical for boundary conditions with unconstrained tangent rotations $\tilde{\theta}_i$ (plates with soft simply supported or free edges), which lead to a strong boundary layer effect. It can be expected that the use of a narrow band of small $\tilde{Q}_{ab-c/d}$ elements along the SS1 or F boundary and crude mesh of \tilde{Q}_{ab-c} elements inside the plate (Fig. 7(c)) will be the optimal solution. One of the advantages of the HT approach is that such refinement is easy to perform. Indeed, since the auxiliary conforming frame functions \tilde{w} , $\tilde{\theta}_x$ and $\tilde{\theta}_y$ need to be defined and the integration of the element matrices performed only along the element boundary, a typical HT p -element subroutine assumes elements with an optional number of sides. This makes it possible to use the combinations of large and small elements, such as shown in Fig. 7(a) and (b), and so to avoid the use of unnecessarily dense FE meshes in regions with a low gradient type of solution.

As in the past for the thin plate elements [8, 41], the planned extensions of the present thick plate elements will include the implementation of curved side geometry and the development of special global or semi-global load terms, $\tilde{u} = \{\tilde{w}, \tilde{\theta}_x, \tilde{\theta}_y\}$, for discontinuous loads (patch loads, line loads, . . . , etc.). The usefulness of the latter resides in the fact that the mesh design and solution accuracy become virtually independent of the loading [13, 41].

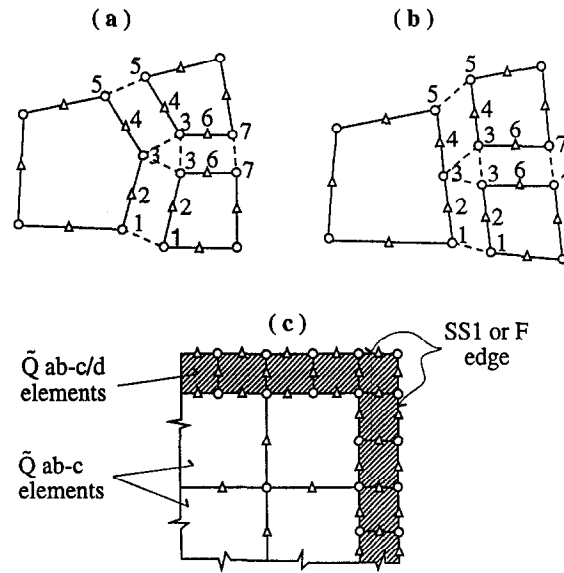


Fig. 7. Local mesh refinement in HT p -element approach (a, b) with application to analysis of boundary layer effect (c).

Acknowledgment

The research reported in this paper has been supported by the Swiss National Science Foundation under Grant No. 20-34601.92.

References

- [1] J. Jirousek and N. Leon, A powerful finite element for plate bending, *Comput. Methods Appl. Mech. Engrg.* 12 (1977) 77–96.
- [2] J. Jirousek, Basis for development of large finite elements locally satisfying all field equations, *Comput. Methods Appl. Mech. Engrg.* 14 (1978) 65–92.
- [3] J. Jirousek and P. Teodorescu, Large finite elements method for the solution of problems in the theory of elasticity, *Comput. Struct.* 15 (1982) 575–587.
- [4] R. Piltner, Special finite elements with holes and internal cracks, *Int. J. Numer. Methods Engrg.* 21 (1985) 1471–1485.
- [5] J. Jirousek and A. Venkatesh, Hybrid-Trefftz planes elasticity elements with p -method capabilities, *Int. J. Numer. Methods Engrg.* 35 (1992) 1443–1472.
- [6] J. Jirousek and Lan Guex, The hybrid-Trefftz finite element model and its application to plate bending, *Int. J. Numer. Methods Engrg.* 23 (1986) 651–693.
- [7] J. Jirousek, Hybrid-Trefftz plate bending elements with p -method capabilities, *Int. J. Numer. Methods Engrg.* 24 (1987) 1367–1393.
- [8] J. Jirousek and A. Venkatesh, Implementation of curvilinear geometry into p -version HT plate elements, *Int. J. Numer. Methods Engrg.* 28 (1989) 431–443.
- [9] G.M. Vörös and J. Jirousek, Application hybrid-Trefftz finite element model to thin shell analysis, *Proc. European Conf. on New Advances in Comput. Struct. Mech.*, pp. 547–554, Giens (Var), France, 1991.
- [10] A. Wróblewski, A.P. Zieliński and J. Jirousek, Hybrid-Trefftz p -elements for 3D axisymmetric problems of elasticity, in: Ch. Hirsch, O.C. Zienkiewicz and E. Oñate, eds., *Numerical Methods in Engineering '92* (Elsevier, Amsterdam, 1992) 801–810.
- [11] A. Wróblewski and J. Jirousek, Application of hybrid-Trefftz p -elements to stress analysis in shafts, *Proc. XI Polish Conference on Comp. Meth. in Mech.*, vol. 2, pp. 983–990, Kielce-Cedzyna, Poland, 1993.
- [12] A.P. Zieliński and O.C. Zienkiewicz, Generalized finite element analysis with T-complete solution functions, *Int. J. Numer. Methods Engrg.* 21 (1985) 509–528.
- [13] J. Jirousek, A. Venkatesh, A.P. Zielinski and H. Rabemantantsoa, Comparative study of p -extensions based on conventional assumed displacement and hybrid-Trefftz FE models, *Comput. Struct.* 46 (1993) 261–278.
- [14] J. Petrolito, Hybrid-Trefftz quadrilateral elements for thick plate analysis, *Comput. Methods Appl. Mech. Engrg.* 78 (1990) 331–351.

- [15] J. Jirousek, A. Wróblewski and B. Szybiński, A new 12DOF quadrilateral element for analysis of thick and thin plates, *Int. J. Numer. Methods Engrg.* 38 (1995) 2619–2638.
- [16] Z. Xu, A simple and efficient triangular finite element for plate bending, *Acta Mechanica Sinica* 2 (1986) 185–192.
- [17] M.A. Aminpour, A 4-node assumed stress hybrid shell element with rotational degrees of freedom, NASA CR-4279, 1990.
- [18] Z. Xu, A thick-thin triangular element, *Int. J. Numer. Methods Engrg.* 33 (1992) 963–973.
- [19] M.A. Aminpour, Direct formulation of a hybrid 4-node shell element with drilling degrees of freedom, *Int. J. Numer. Methods Engrg.* 35 (1992) 997–1013.
- [20] O.C. Zienkiewicz, Z. Xu, L.F. Zeng, A. Samuelson and N.E. Wiberg, Linked interpolation for Reissner–Mindlin plate elements: Part I—A simple quadrilateral, *Int. J. Numer. Methods Engrg.* 36 (1993) 3043–3056.
- [21] R.L. Taylor and F.A. Auricchio, Linked interpolation for Reissner–Mindlin plate elements: Part II—A simple triangle, *Int. J. Numer. Methods Engrg.* 36 (1993) 3057–3066.
- [22] A. Ibrahimbergovic, Quadrilateral finite elements for analysis of thick and thin plates, *Comput. Methods Appl. Mech. Engrg.* 110 (1993) 195–209.
- [23] I. Herrera, *Boundary Methods—An Algebraic Theory* (Pitman Advanced Publishing Program, 1984).
- [24] E. Reissner, The effect of shear deformation on the bending of elastic plates, *J. Appl. Mech.* 12 (1945) 69–76.
- [25] R.D. Mindlin, Influence of rotatory inertia and shear in flexural motion of isotropic elastic plates, *J. Appl. Mech.* 18 (1951) 31–38.
- [26] J. Jirousek, Variational formulation of two complementary hybrid-Trefftz FE models, *Comm. Appl. Numer. Methods* 9 (1993) 837–845.
- [27] Hu, Hai-chang, On some problems of the antisymmetrical small deflection of isotropic sandwich plate (in Chinese), *Acta Mechanica Sinica* 6 (1963) 53–60.
- [28] G.A. Korn and T.M. Korn, *Mathematical Handbook for Scientists and Engineers* (McGraw-Hill, New York, 1968).
- [29] H. Reissmann, *Elastic Plates: Theory and Applications* (Wiley, New York, 1988).
- [30] V. Panc, *Theories of Elastic Plates* (Noordhoff, Leiden, 1975).
- [31] J. Jirousek, Structural analysis program SAFE—special features and advanced finite element models, *Adv. Eng. Software* 7 (1985) 68–76.
- [32] M. Mukhopadhyay, Analysis of plates using isoparametric quadratic elements—shear, rection, patch loading and some convergence studies, *Comput. Struct.* 17 (1983) 587–597.
- [33] J. Jirousek and A. Boubergnig, A contribution of evaluation of shear forces and reactions of Mindlin plates using isoparametric elements, *Comput. Struct.* 19 (1984) 793–800.
- [34] J. Jirousek, Comment on evaluation of shear forces and reactions from transverse shear deformations by using isoparametric quadratic Mindlin plate elements, *Comput. Struct.* 19 (1984) 899–903.
- [35] T.J.R. Hughes and L.P. Franca, Convergence of transverse shear stress in the finite element analysis, *Comm. Appl. Numer. Methods* 4 (1988) 185–187.
- [36] S. Ahmad, B.M. Irons and O.C. Zienkiewicz, Analysis of thick and thin shell structures by curved finite elements, *Int. J. Numer. Methods Engrg.* 2 (1970) 419–451.
- [37] O.C. Zienkiewicz, *The Finite Element Method*, 3rd edition (McGraw-Hill, London, 1977).
- [38] E. Hinton and J. Campbell, Local and global smoothing of discontinuous finite element functions using a least square method, *Int. J. Numer. Methods Engrg.* 8 (1974) 461–480.
- [39] T. Kant and E. Hinton, Mindlin plate analysis by segmentation method, *J. Engrg. Mech. ASCE* 109 (1983) 537–556.
- [40] J. Jirousek and A. Venkatesh, A simple stress error estimator for hybrid Trefftz p -version elements, *Int. J. Numer. Methods Engrg.* 28 (1989) 211–236.
- [41] A. Venkatesh and J. Jirousek, Accurate FE analysis of thin plates under concentrated loading, IREM Int. Report 89/6, LSC—Swiss Federal Institute of Technology, Lausanne, 1989.